Thermo-Hydro-Mechanical Modeling of Damage in Unsaturated Porous Media: Theoretical Framework and Numerical Study of the EDZ

C. Arson[1], B. Gatmiri[2]
1. Texas A&M University, College Station, Texas
2. Ecole Nationale des Ponts et Chaussées, France

The damage model presented in this article (named "THHMD" model) is dedicated to non-isothermal unsaturated porous media. It is formulated by means of three independent strain state variables, which are the thermodynamic conjugates of net stress, suction and thermal stress. The damage variable is a second-order tensor. Stress/strain relationships are derived from Helmholtz free energy, which is assumed to be the sum of damaged elastic potentials and "crack-closure energies". Damage is assumed to grow with tensile strains due to net stress, with pore shrinkage due to suction and with thermal dilatation. Specific conductivities are introduced to account for the effects of cracking on the intensification and on the orientation of liquid water and vapor flows. These conductivities depend on damage and on internal length parameters. The mechanical aspects of the THHMD model are validated by comparing the results of a triaxial compression test to experimental measurements found in the literature. Parametric studies of damage are performed on three different heating problems related to nuclear waste disposals. Several types of loading and boundary conditions are investigated. The thermal damage potential is thoroughly studied. The THHMD model is expected to be a useful tool in the assessment of the Excavation Damaged Zone (EDZ), especially in the vicinity of nuclear waste repositories.

Keywords. Poromechanics, Continuum Damage Mechanics, unsaturated rock, thermo-hydro-mechanical couplings, multi-phase transfers, Finite Element Method, heating test, nuclear waste repository, Excavation Damaged Zone

1. INTRODUCTION

Many geomaterials, like tuff, granite or clay rock, are brittle. The Excavation Damaged Zone (EDZ) generated in such media has to be assessed in order to design safe underground facilities. Porous host rocks contain various pore fluids, which makes engineering problems very complex. Capillary effects change the behavior of the bedrock. In addition, temperature gradients may induce phase changes, which influence transfer kinetics. The stakes are particularly high in nuclear waste repositories, provided that radioactive packages behave as heating sources [11, 57, 59, 75]. Poromechanics and Continuum Damage Mechanics are two well-identified scientific fields. But it is still hard to combine both theories to study cracking in porous media [2].

On the one hand, Continuum Damage Mechanics provides a theoretical framework to develop damage and fatigue models for solids [54]. In micromechanical models, stresses are assumed to be redistributed due to a decrease of the effective material area. Stress-strain relationships are thus written in terms of effective variables. Effective stress is the stress which develops in the fictive undamaged counterpart of the system [21]. The proper definition of effective stress requires the use of a fourth-order operator [44]. Effective stresses describe mechanical damage effects rather than cracking evolution. Damage growth itself is often associated to the development of tensile strains [60]. In phenomenological damage models, the brittle behavior law is derived from the postulated expression of a thermodynamic potential [16, 17, 44, 58, 65, 73]. Generally speaking, damage represents the effects of micro-cracking on the macroscopic behavior of a medium. That is the reason why damage is non-local [7]. As a consequence, softening constitutive models often need to be regularized before being used in a numerical code. Either a differential [6, 21, 53, 62] or an integral formulation [8, 9, 22, 49] can be adopted. Micro-structure enriched models also avoid localization problems. Up to now, they are more common in elasto-plasticity than in damage mechanics [14, 77], even if some models were developed for isotropic damage [29]. A full representation of the thermo-hydro-mechanical behavior of the host rock requires the coupling of all degrees of freedom. Most of the existing models tend to separate problems, by modeling mechanical damage on the one hand, and the elastic unsaturated behavior on the other hand. Formulations based on Bishop's effective stress take damage and capillary effects into account, but damage remains uncoupled from fluid effects [12, 48, 70, 71].

Only a few damage models proposed for unsaturated porous media have been extended to non-isothermal conditions. Gawin et al. [35, 36] modeled damage in unsaturated concrete subjected to temperature changes. Even if two scalar damage variables are introduced (to distinguish the response of the material in traction and in compression), damage is assumed to be isotropic. Damage grows with total strains, which merge hygro-thermal and mechanical strains. The model of degraded mechanical stiffness has recently been extended to thermo-mechanical couplings induced by hygro-chemical processes [37]. Schrefler then provided a general framework to study isotropic damage in deformable unsaturated porous media subjected to hygro-thermal changes [69]. Applications have recently been found in cementitious materials [51, 52, 63, 38].

On the other hand, transfers in cracked porous media were extensively modeled by fracture network theories. The differences between such models lie in the number of represented continua and in the way fluid exchanges between media are taken into account. In multimodal models [25], all kinds of voids are assumed to connect and to form a unique fracture network. In a Representative Elementary Volume (REV), the pore pressure of the fluid is thus assumed to be homogeneous. Only one balance equation is needed to model fluid transfers in the pores of the intact matrix on the one hand, and in the micro-cracks on the other hand. In multi-continua models [40, 61, 79], several networks are assumed to drive fluid flows separately, but not always independently. Each continuum is thus characterized by its own pressure head. Richard's equations are coupled. The coupling terms represent the fluid exchanges which may occur at the boundary between two media (between the porous matrix and the cracks network, for instance). A penetration time can be defined [67, 80], in order to indicate when suction equilibrium occurs, and consequently, when it is possible to consider one single pressure head variable for the whole REV. Fracture network models remain focused on fluid flow problems, and do not represent the mechanical behavior of the cracked porous material.

The damage model presented in this article (named "THHMD" model) is dedicated to non-isothermal unsaturated porous media. It is designed to represent the combined effects of mechanical, capillary and thermal cracking. The Representative Elementary Volume is assumed to be constituted of a solid skeleton and of a porous network. The pores are filled with liquid

water and gas. Due to pressure and temperature changes, water may evaporate. Gas is thus a mixture of dry air and vapor. Section 2 provides the main assumptions founding the THHMD model. In Section 3, the modeling approach is presented in detail, the state laws are established and the damage evolution law is expressed. All transfer equations are given in Section 4. The emphasis is put on the introduction of damage in water permeability and vapor diffusivity. Balance equations for all constituents (solid skeleton, water, air, heat) are recalled in Section 5. The numerical applications presented Section 6 are mainly focused on the effects of thermal damage. The first one validates the mechanical aspects of the THHMD model. The second one is a simplified nuclear waste repository model, involving thermal and mechanical degrees of freedom only. The third one is a heating test performed in a tank filled with unsaturated compacted clay. The fourth one is a full-scale heating test performed in an experimental nuclear waste repository.

2. MAIN MODELING ASSUMPTIONS

2.1. Choice of the Damage Variable

The damage model used in this study (named "THHMD model") is based on energetic computations. The proposed formulation does not aim at representing the geometry of a cracks network at the current stress state. Void nucleation and cracks coalescence induce energy dissipation. A damage variable is introduced to compute the corresponding loss of elastic deformation energy at the scale of a Representative Elementary Volume (REV). If a volume V_{REV} of material is damaged by N non-interacting cracks (this assumption is justified in the following), the variation of elastic deformation energy may be averaged as [50]:

$$\Delta W^e = \frac{1}{2V_{REV}} \sum_{i=1}^{N} \mathbf{n^i} \cdot \sigma \cdot < \mathbf{b} >^{\mathbf{i}} S^i \tag{1}$$

in which $\mathbf{n^i}$ is the vector normal to the i^{th} crack plane. $< \mathbf{b} >^{\mathbf{i}}$ is the average displacement discontinuity vector which characterizes the opening of the i^{th} fissure. S^i is the surface of the i^{th} crack damaging the material volume V. σ_{kl} is the macroscopic stress exerted on the cracked material at the scale of the REV. In two dimensions, the average crack opening displacement $< \mathbf{b} >^{\mathbf{i}}$ is collinear to the macroscopic traction vector $\mathbf{n^i} \cdot \sigma$. In three dimensions, the opening vector has a shearing component, which is collinear to

$(\mathbf{n^i} \cdot \sigma \cdot \mathbf{n^i})\mathbf{n^i} - \mathbf{n^i} \cdot \sigma$. If the cracks do not interact, the variation of elastic deformation energy originated by damage thus depends on a fourth order tensor. However, as mentioned by Kachanov [50], the latter has a negligible influence on the loss of energy, which may thus be approximated as:

$$\Delta W_e = \frac{8(1-\nu_0^2)}{3(1-\nu_0/2)E_0} \left(\sigma_{ij}\sigma_{jl}\right) D_{m_{li}} \tag{2}$$

in which E_0 and ν_0 are the Young's modulus and Poisson's ratio of the intact material, respectively. $D_{m_{ij}}$ is the second-order crack-density tensor. In this study, the damage variable (noted Ω_{ij}) is defined as the spectral decomposition of $D_{m_{ij}}$:

$$\mathbf{\Omega} = \sum_{I=1}^{3} d^I \mathbf{n^I} \otimes \mathbf{n^I} \tag{3}$$

d^I and $\mathbf{n^I}$ are the I^{th} eigenvalue and I^{th} eigenvector of the crack density tensor $D_{m_{ij}}$, respectively. With this definition of damage, the geometric representation of micro-cracks is homogenized at the scale of the REV. Each micro-crack is assumed to belong to one crack family, characterized by a crack-plane orientation. The three principal cracks' orientations define three crack families. At the scale of the REV, these three families are represented by three equivalent cracks (See Figure 1). The I^{th} equivalent crack is characterized by its volumetric fraction d^I and by the vector $\mathbf{n^I}$, normal to the I^{th} equivalent crack plane. The equivalent cracks are assumed to be penny-shaped, with a radius r^I and an opening e^I. A linear dilatancy rule relates r^I and e^I [72]:

$$d^I = \frac{1}{V_{REV}} e^I \pi \left(r^I\right)^2, \qquad \delta e^I = \chi \, \delta r^I \tag{4}$$

In situ observations show that the Excavated Damaged Zone (EDZ) surrounding deep galleries is constituted of non-connected fractures families. At a smaller scale, non-connected cracks are also observed in damaged rock samples [10]. It is thus justified to define a Representative Elementary Volume, at the scale of which material parameters are homogenized under the assumption of cracks non-interaction. As demonstrated above, this common assumption [41] enables the computation of energy loss by means of a second-order damage tensor. Moreover, assuming that cracks do not connect does not imply that they do not constitute a flow path. Cracks are larger than

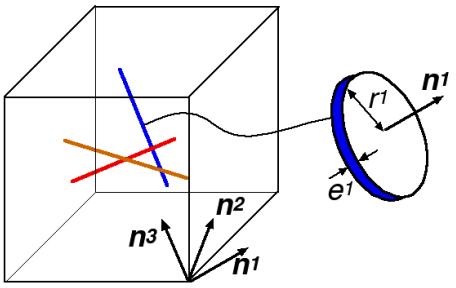

Figure 1: Equivalent Cracks in a 3D REV.

the natural pores of the matrix. As a result, each crack is connected to the natural porous network, and fluids flow continuously through this network made of natural pores and cracks [55, 56].

2.2. Formulation in Independent Strain State Variables

The THHMD model is dedicated to unsaturated porous media. In the following, it is understated that the pores of the solid matrix are filled with liquid water and a gaseous mixture of dry air and vapor. In Continuum Damage Mechanics, almost all models developed for unsaturated media are based on the concept of Bishop's effective stress [12, 48, 71]. In such theoretical frames, some important aspects of the behaviour of unsaturated soils, like wetting collapse, cannot be represented [28, 46]. Noting p_w and p_g the pore pressures of liquid water and gas respectively, and noting δ_{ij} the second-order identity tensor, net stress is defined as $\sigma"_{ij} = \sigma_{ij} - p_g\delta_{ij}$, and suction is defined as $s = p_g - p_w$. Assuming that deformations are small and that the solid phase is incompressible, the Inequality of Clausius-Duhem for an open, damaged, non-isothermal, unsaturated system writes [19]:

$$\sigma"_{ij}\,\delta\epsilon_{ji} + s\delta\left(-nS_w\right) - \eta\delta T - \delta\Psi_s\left(\epsilon_{pq}, nS_w, T, \Omega_{pq}\right) \geq 0 \qquad (5)$$

in which ϵ_{ij} is the linearized strain tensor, n is porosity, S_w is the degree of saturation of liquid water, η is entropy, and Ψ_s is Helmholtz volumetric free energy. The constitutive model may be expressed in terms of net stress, suction and temperature, which are thermodynamically independent. The THHMD model is formulated in net stress, suction and thermal stress (p_T). Thermal stress is a scalar stress variable depending on temperature only. Net stress, suction and thermal stress are thus thermodynamically independent,

and are conjugate to independent strain state variables:

$$\begin{cases} \sigma"_{ij} \longleftrightarrow \epsilon_{Mij} \\ s \longleftrightarrow \epsilon_{Sv} \\ p_T \longleftrightarrow \epsilon_{Tv} \end{cases} \tag{6}$$

ϵ_{Mij}, ϵ_{Sv} and ϵ_{Tv} are respectively called mechanical strains, capillary strains and thermal strains. These latter are thermodynamically independent, so that the incremental total strain tensor $d\epsilon_{ij}$ may be decomposed as:

$$d\epsilon_{ij} = \left(d\epsilon^e_{M_{ij}} + d\epsilon^d_{M_{ij}}\right) + \frac{1}{3}\left(d\epsilon^e_{Sv} + d\epsilon^d_{Sv}\right)\delta_{ij} + \frac{1}{3}\left(d\epsilon^e_{Tv}\,\delta_{ij} + d\epsilon^d_{Tv}\right)\delta_{ij} \tag{7}$$

in which e and d subscripts refer to elastic and inelastic components, respectively. Thermal strains are related to temperature by a damaged thermal expansion coefficient $\alpha^*(\Omega_{pq})$ (in ${}^oC^{-1}$), depending on damage and on a reference thermal expansion coefficient α^*_0. In an intact material, thermal deformations are elastic, so that:

$$d\epsilon^e_{Tv} = \alpha^*_0\, dT \tag{8}$$

In the same way, thermal stress is related to thermal deformations by a thermal modulus $\beta_T(\Omega_{pq})$ (in Pa), depending on damage and on a reference modulus β^0_T. In an intact material:

$$d\epsilon^e_{Tv} = \frac{1}{\beta^0_T}\, dp_T \tag{9}$$

In an intact porous medium, the increments of temperature and thermal stress are thus simply related by:

$$dp_T = \beta^0_T\, \alpha^*_0\, dT \tag{10}$$

It is assumed that the constitutive relationship between temperature and the thermal stress does not depend on the state of damage, so that the relation stated in equation 10 even holds if damage grows. As a result:

$$dp_T = \beta_T(\Omega_{pq})\ \alpha^*(\Omega_{pq})\, dT \tag{11}$$

The expression of the damaged thermal modulus $\beta_T(\Omega_{pq})$ as a function of the reference modulus β_T^0 and in function of damage will be computed in the following section. With the choice of independent strain state variables described in equation 6, the Inequality of Clausius-Duhem writes [3, 5]:

$$\sigma"_{ij}\, d\epsilon_{M_{ji}} + s\, d\epsilon_{Sv} + p_T\, d\epsilon_{Tv} - d\Psi_s\left(\epsilon_{M_{pq}}, \epsilon_{Sv}, \epsilon_{Tv}, \Omega_{pq}\right) \geq 0 \tag{12}$$

The corresponding conjugation relations are:

$$\begin{cases} \sigma"_{ij} = \frac{\partial \Psi_s\left(\epsilon_{M\,pq}, \epsilon_{Sv}, \epsilon_{Tv}, \Omega_{pq}\right)}{\partial \epsilon_{M\,ij}} \\ s = \frac{\partial \Psi_s\left(\epsilon_{M\,pq}, \epsilon_{Sv}, \epsilon_{Tv}, \Omega_{pq}\right)}{\partial \epsilon_{Sv}} \\ p_T = \frac{\partial \Psi_s\left(\epsilon_{M\,pq}, \epsilon_{Sv}, \epsilon_{Tv}, \Omega_{pq}\right)}{\partial \epsilon_{Tv}} \\ Y_{dij} = -\frac{\partial \Psi_s\left(\epsilon_{M\,pq}, \epsilon_{Sv}, \epsilon_{Tv}, \Omega_{pq}\right)}{\partial \Omega_{ij}} \end{cases} \tag{13}$$

Y_{dij} is conjugate to damage. The product of Y_{dij} by damage is an energy release rate. Y_{dij} is named "damage affinity" in the following. The THHMD model is based on a postulate on the expression of Helmholtz free energy. The following paragraph gives a physical justification of the expression chosen in this formulation.

2.3. Concept of Equivalent Mechanical State

In the real mechanical state, N micro-stresses τ_{ij}^K (K=1,...,N) open N micro-cracks in the REV. According to the definition of the damage variable, the micro-cracks are represented by three equivalent penny-shaped cracks characterized by their normal vector $\mathbf{n^I}$ (I=1,2,3). In the same way, the micro-stresses are gathered in three principal families, according to their orientation. The principal stresses are perpendicular to the equivalent crack planes. The corresponding equivalent stress field τ_{ij} is thus defined as:

$$\tau_{ij} = \sum_{I=1}^{3}\left(\tau^I\, n^I{}_i\, n^I{}_j\right) \tag{14}$$

The opening of the I^{th} equivalent crack grows with the I^{th} equivalent stress eigenvalue τ^I. In other words, d^I grows with τ^I. Assuming that the evolution

law is linear and that the growth coefficient is the same in all directions [74] leads to:

$$\tau_{ij} \;=\; g\,\Omega_{ij} \tag{15}$$

in which g represents the resistance to damage (in Pa). The equivalent mechanical state is defined as the state in which the damaged material may be considered elastic. In other words, in the equivalent state, the material has a lower rigidity than the intact material, but strains remain reversible. Crack openings are thus accounted for by the stress field perturbation induced by the micro-stresses τ_{ij}^{K}. As a consequence, in the equivalent mechanical state, a damaged material is subjected to an equivalent stress $\widetilde{\sigma}_{ij}$, defined as the sum of the far field stress σ_{ij} and of the equivalent stress τ_{ij} [5, 74]:

$$\widetilde{\sigma}_{ij} \;=\; \sigma_{ij} \;+\; \tau_{ij} \tag{16}$$

In the equivalent mechanical state, stresses are conjugate to deformations by a damaged elastic potential. Assuming that strains and damage are the same in the equivalent and in the real mechanical states [74], the conjugation relations for an isothermal solid turn to be:

$$\left\{\begin{array}{l} \Psi_e^*(\widetilde{\sigma}_{pq},\Omega_{pq}) + \Psi_e(\epsilon_{pq},\Omega_{pq}) \;=\; \widetilde{\sigma}_{ij}\,\epsilon_{ji} \\ \\ \epsilon_{ij} \;=\; \frac{\partial \Psi_e^*(\widetilde{\sigma}_{pq},\Omega_{pq})}{\partial \widetilde{\sigma}_{ij}}, \quad \widetilde{\sigma}_{ij} \;=\; \frac{\partial \Psi_e(\epsilon_{pq},\Omega_{pq})}{\partial \epsilon_{ij}} \end{array}\right. \tag{17}$$

in which * denotes the partial Legendre transform relative to strains. Noting that the far-field stress σ_{ij} is conjugate to strains by Helmholtz free energy $\Psi_s(\epsilon_{pq},\Omega_{pq})$ [54], the resulting expression of Helmholtz free energy for an isothermal solid is:

$$\Psi_s(\epsilon_{pq},\Omega_{pq}) \;=\; \Psi_e(\epsilon_{pq},\Omega_{pq}) - \tau_{ij}\,\epsilon_{ji} \;=\; \frac{1}{2}\epsilon_{ji}\,D_{eijkl}\,(\Omega_{pq})\;\epsilon_{lk} - g\Omega_{ij}\,\epsilon_{ji} \tag{18}$$

in which $D_{eijkl}\,(\Omega_{pq})$ is the fourth-order rigidity tensor, depending on damage and on a reference stiffness tensor D^0_{eijkl} characterizing the intact material. The computation of $D_{eijkl}\,(\Omega_{pq})$ is detailed in the following section. The stress applied to the REV is obtained by deriving the free energy 18:

$$\sigma_{ij} \;=\; \frac{\partial \Psi_s(\epsilon_{pq},\Omega_{pq})}{\partial \epsilon_{ij}} \;=\; D_{eijkl}\,(\Omega_{pq})\;\epsilon_{lk} \;- g\Omega_{ij} \tag{19}$$

If cracks open due to a tensile load, a bare unloading to $\sigma_{ij} = 0$ will not close the cracks ($\epsilon_{ij} \neq 0$). To close the cracks, an additional compression

$(-g\Omega_{ij})$ would be necessary. In other words, the term $-g\Omega_{ij}\epsilon_{ji}$ in equation 18 is the energy that would be required to close remaining openings. It will be referred to as "crack-closure energy" in the following. It represents the existence of residual strains. Note that crack closure is not accounted for in this model. Residual openings are thus considered irreversible.

3. STRESS/STRAIN RELATIONSHIPS

3.1. Expression of Helmholtz Free Energy

The free energy of the non-isothermal porous REV is assumed to have the same form as for the solid (equation 18). The degraded elastic potential and the"crack-closure energy" thus have three terms, each of which referring to one of the independent stress state variable:

$$\begin{aligned}
&\Psi_s(\epsilon_{Mpq}, \epsilon_{Sv}, \epsilon_{Tv}, \Omega_{pq}) \; = \\
&\tfrac{1}{2}\,\epsilon_{Mji}\,D_{eijkl}\,(\Omega_{pq})\;\epsilon_{Mlk} \;+\; \tfrac{1}{2}\,\epsilon_{Sv}\,\beta_s\,(\Omega_{pq})\;\epsilon_{Sv} \;+\; \tfrac{1}{2}\,\epsilon_{Tv}\,\beta_T\,(\Omega_{pq})\;\epsilon_{Tv} \\
&-g_M\,\Omega_{ij}\,\epsilon_{Mji} \;-\; \tfrac{g_S}{3}\,\Omega_{ij}\,\delta_{ji}\,\epsilon_{Sv} \;-\; \tfrac{g_T}{3}\,\Omega_{ij}\,\delta_{ji}\,\epsilon_{Tv}
\end{aligned} \tag{20}$$

in which $\beta_s\,(\Omega_{pq})$ is a capillary modulus (in Pa), depending on damage and on a reference modulus β_s^0, characterizing the intact material. $\beta_T\,(\Omega_{pq})$ has already been defined in equations 9-11. g_M (respectively g_S and g_T) represents the resistance of the material to mechanical (respectively capillary and thermal) cracking (in Pa).

3.2. Damaged Rigidities

The concept of effective stress, commonly used in Continuum Damage Mechanics [44, 54], is extended to the three stress state variables used in the THHMD model. The operator of Cordebois and Sidoroff [18] is used in order to define the damaged effective stress variables $\widehat{\sigma"}_{ij}$, $\widehat{s}$, $\widehat{p_T}$ [3]:

$$\left\{\begin{array}{l}
\widehat{\sigma"}_{ij} \;=\; (\delta-\Omega)^{-1/2}_{ik}\;\sigma"_{kl}\;(\delta-\Omega)^{-1/2}_{lj} \\
\widehat{s} \;=\; \frac{s}{3}\;(\delta-\Omega)^{-1}_{ij}\;\delta_{ji} \\
\widehat{p_T} \;=\; \frac{p_T}{3}\;(\delta-\Omega)^{-1}_{ij}\;\delta_{ji}
\end{array}\right. \tag{21}$$

The damaged rigidities are determined by application of the Principle of Equivalent Elastic Energy, which states that the elastic energy of the damaged REV subjected to $\sigma"_{ij}$, s and p_T is equal to the elastic energy of a

fictitious intact REV subjected to $\widehat{\sigma"}_{ij}$, $\widehat{s}$ and $\widehat{p_T}$. If $M_{ijkl}(\Omega_{pq})$ denotes the operator of Cordebois and Sidoroff, we thus have:

$$\begin{cases} D_{eijkl}(\Omega_{pq}) = M(\Omega_{pq})^{-1}_{ijnm} \; D^0_{emnst} \, M(\Omega_{pq})^T_{tskl} \\ \beta_s(\Omega_{pq}) = \frac{9\beta_s^0}{\left[(\delta-\Omega)^{-1}_{ij}\,\delta_{ji}\right]^2} \\ \beta_T(\Omega_{pq}) = \frac{9\beta_T^0}{\left[(\delta-\Omega)^{-1}_{ij}\,\delta_{ji}\right]^2} \end{cases} \tag{22}$$

Let's recall that D^0_{eijkl}, β_s^0 and β_T^0 are respectively the mechanical stiffness tensor, the capillary modulus and the thermal modulus of the intact material. Following the approach of Gatmiri [30, 31, 32, 33, 34], capillary and thermal strains are assumed volumetric, so that the conjugate stress variables (respectively suction and thermal stress) are also scalars. As a consequence, capillary and thermal stress/strain relationships are expressed by means of scalar moduli. The damaged capillary and thermal moduli are computed from the isotropic part of the damage tensor. Even if the damage tensor may be anisotropic, the cracking effects on β_s and β_T are isotropic. The authors intend to account for damaged-induced anisotropy in the thermal expansion properties in further developments.

3.3. State Laws

At this stage, it is easy to deduce the increments of the elastic strain components. For a fixed damage state:

$$\begin{cases} d\epsilon_{M}{}^{e}_{ij} \;=\; D_{eijkl}(\Omega_{pq})^{-1} \; d\sigma"_{lk} \\ d\epsilon^e_{Sv} \;=\; \frac{ds}{\beta_s(\Omega_{pq})} \\ d\epsilon^e_{Tv} \;=\; \frac{dp_T}{\beta_T(\Omega_{pq})} \end{cases} \tag{23}$$

The incremental state laws result from the combination of equations 13 and 20:

$$\begin{cases} d\sigma"_{ij} \;=\; D_{eijkl}(\Omega_{pq}) \; d\epsilon_{Mlk} \;+\; \left(\frac{\partial D_{eijkl}(\Omega_{pq})}{\partial \Omega_{mn}}\,\epsilon_{Mnm}\right) d\Omega_{lk} \;-\; g_M \, d\Omega_{ij} \\ ds \;=\; \beta_s(\Omega_{pq}) \; d\epsilon_{S_v} \;+\; \left(\frac{\partial \beta_s(\Omega_{pq})}{\partial \Omega_{ij}}\,\epsilon_{Sv}\right) d\Omega_{ji} \;-\; \frac{g_S}{3}\,\delta_{ij}\,d\Omega_{ji} \\ dp_T \;=\; \beta_T(\Omega_{pq}) \; d\epsilon_{T_v} \;+\; \left(\frac{\partial \beta_T(\Omega_{pq})}{\partial \Omega_{ij}}\,\epsilon_{Tv}\right) d\Omega_{ji} \;-\; \frac{g_T}{3}\,\delta_{ij}\,d\Omega_{ji} \end{cases} \tag{24}$$

The expressions of the incremental inelastic strains are obtained by combining equations 23 and 24.

$$\begin{cases} d\epsilon_{M}{}^{d}_{ij} \;=\; -\left(D_{eklhg}\,(\Omega_{pq})^{-1}\;\frac{\partial D_{eghij}(\Omega_{pq})}{\partial \Omega_{mn}}\,\epsilon_{Mnm}\right)\,d\Omega_{lk} \;+ g_M\,D_{eijkl}\,(\Omega_{pq})^{-1}\;d\Omega_{lk} \\ d\epsilon^{d}_{S_v} \;=\; -\left(\frac{\epsilon_{Sv}}{\beta_s(\Omega_{pq})}\,\frac{\partial \beta_s(\Omega_{pq})}{\partial \Omega_{ij}}\right)\,d\Omega_{ji} \;+\; \frac{g_S}{3\,\beta_s(\Omega_{pq})}\,\delta_{ij}\,d\Omega_{ji} \\ d\epsilon^{d}_{T_v} \;=\; -\left(\frac{\epsilon_{Tv}}{\beta_T(\Omega_{pq})}\,\frac{\partial \beta_T(\Omega_{pq})}{\partial \Omega_{ij}}\right)\,d\Omega_{ji} \;+\; \frac{g_T}{3\,\beta_T(\Omega_{pq})}\,\delta_{ij}\,d\Omega_{ji} \end{cases} \tag{25}$$

In the right-hand side of expressions 25, the first term is reversible, and represents the increase of strain rate when stiffness gets lower due to damage growth. The second term is irreversible, and represents the remaining crack openings mentioned in the paragraph related to the equivalent mechanical state. Incremental irreversible strains are thus given by:

$$\begin{cases} d\epsilon_{M}{}^{irr}_{ij} \;=\; g_M\,D_{eijkl}\,(\Omega_{pq})^{-1}\;d\Omega_{lk} \\ d\epsilon^{irr}_{S_v} \;=\; \frac{g_S}{3\,\beta_s(\Omega_{pq})}\,\delta_{ij}\,d\Omega_{ji} \\ d\epsilon^{irr}_{T_v} \;=\; \frac{g_T}{3\,\beta_T(\Omega_{pq})}\,\delta_{ij}\,d\Omega_{ji} \end{cases} \tag{26}$$

3.4. Damage Evolution Law

$d\epsilon_{M}{}^{d}_{ij}$, $d\epsilon^{d}_{S_v}$ and $d\epsilon^{d}_{T_v}$ depend on the increment of damage (equation 25), which is computed as:

$$d\Omega_{ij} \;=\; d\lambda_d\,\frac{\partial f_d\left(Y_{dpq},\Omega_{pq}\right)}{\partial Y_{dij}} \tag{27}$$

in which $d\lambda_d$ is the damage multiplier, and $f_d\left(Y_{dpq},\Omega_{pq}\right)$ is a damage evolution function, depending on damage affinity Y_{dij}. The latter is computed by combining equations 13 and 20:

$$\begin{aligned} Y_{dij} \;=\; & -\tfrac{1}{2}\,\epsilon_{Mlk}\,\frac{\partial D_{eklij}(\Omega_{pq})}{\partial \Omega_{mn}}\,\epsilon_{Mnm} \;-\; \tfrac{1}{2}\,\epsilon_{S_v}\,\frac{\partial \beta_s(\Omega_{pq})}{\partial \Omega_{ij}}\,\epsilon_{S_v} \;-\; \tfrac{1}{2}\,\epsilon_{T_v}\,\frac{\partial \beta_T(\Omega_{pq})}{\partial \Omega_{ij}}\,\epsilon_{T_v} \\ & +g_M\,\epsilon_{Mij} \;+\; \tfrac{g_S}{3}\epsilon_{S_v}\,\delta_{ij} \;+\; \tfrac{g_T}{3}\epsilon_{T_v}\,\delta_{ij} \end{aligned} \tag{28}$$

A simple damage evolution function is chosen:

$$f_d\left(Y_{dpq},\Omega_{pq}\right) \;=\; \sqrt{\frac{1}{2}\,Tr\left(Y^{+}_{d_1\,ij}\,Y^{+}_{d_1\,ji}\right)} \;-\; C_0 \;-\; C_1\delta_{ij}\,\Omega_{ji} \tag{29}$$

in which:

$$Y^{+}_{d1\,ij} \;=\; g_M\,\epsilon^{+}_{Mij} \;+\; \frac{g_S}{3}\epsilon^{-}_{Sv}\delta_{ij} \;+\; \frac{g_T}{3}\epsilon^{+}_{Tv}\delta_{ij} \tag{30}$$

This type of damage growth criterion is pretty commonly used [15, 41, 24, 42, 70]. C_0 is the initial damage affinity rate which is necessary to trigger damage. C_1 controls the damage increase rate. $Y^{+}_{d1\,ij}$ represents the tensile forces applied on the REV and resulting in irreversible crack openings. Damage may only grow when the solid skeleton is subjected to tensile strains. These latter may be due to a tensile mechanical loading applied on the REV ($g_M\,\epsilon^{+}_{Mij}$), to a pore shrinkage due to a suction increase in the REV ($\frac{g_S}{3}\epsilon^{-}_{Sv}\delta_{ij}$), or to a thermal dilatation of the grains related to a tensile thermal strain of the REV ($\frac{g_T}{3}\epsilon^{+}_{Tv}\delta_{ij}$). As a result, three possible origins of damage are accounted for. Mechanical damage is controlled by $g_M\,\epsilon^{+}_{Mij}$, capillary damage is controlled by $\frac{g_S}{3}\epsilon^{-}_{Sv}\delta_{ij}$, and thermal damage is controlled by $\frac{g_T}{3}\epsilon^{+}_{Tv}\delta_{ij}$. This means in particular that a bare thermal loading may only produce isotropic damage. But damage-induced anisotropy is accounted for by the mechanical term $g_M\,\epsilon^{+}_{Mij}$. In other words, the Excavation Damaged Zone (EDZ) is modeled by an anisotropic damage tensor. But the damage generated by suction and temperature changes in a gallery is isotropic. Damage due to suction and temperature changes may be anisotropic due to couplings only. For instance, suction and temperature changes may generate anisotropic net stress changes, depending on the boundary conditions. The damage multiplier is computed by using the consistency rule. The incremental damage evolution law turns to be:

$$d\Omega_{ij} \;=\; \frac{Y^{+}_{d_1\,kl}\,dY^{+}_{d_1\,lk}}{C_1\,Tr\left(Y^{+}_{d_1\,pq}\right)}\;\frac{Y^{+}_{d_1\,ij}}{\sqrt{2\,Tr\left(Y^{+}_{d_1\,mn}\,Y^{+}_{d_1\,nm}\right)}} \tag{31}$$

4. TRANSFER EQUATIONS

4.1. Liquid Water Flow

4.1.1. Flow Model in Non-isothermal Unsaturated Conditions

As in the preceding works of Gatmiri [30, 31, 32, 33, 34], the liquid water

flow is assumed to obey an extended Darcy law of the form:

$$V_{wi} \;=\; -K_{wij}\,\nabla_j\left(\Phi_w\right) \tag{32}$$

in which V_{wi} is the liquid water velocity (in m.s^{-1}), K_{wij} is the permeability tensor related to liquid water (in m.s^{-1}), and Φ_w is the total hydraulic potential:

$$\Phi_w \;=\; \Psi_w\left(\theta_w, T\right) \;+\; z \tag{33}$$

The occurrence of the spot height z (in m) makes it possible to take gravitational effects into account. $\Psi_w\left(\theta_w, T\right)$ measures the influence of capillary tension occurring in the pores. It depends on water content (θ_w) and on temperature (T). It is assumed [32, 64] that the capillary and thermal effects may be uncoupled as follows:

$$\Psi_w\left(\theta_w, T\right) \;=\; \frac{\sigma(T)}{\sigma(T_{ref})}\,\Psi_R\left(\theta_w\right) \tag{34}$$

$\Psi_R\left(\theta_w\right)$ is the pore water pressure (in m) at the reference temperature T_{ref}:

$$\Psi_R\left(\theta_w\right) \;=\; \frac{p_w \;- p_g}{\gamma_w} \tag{35}$$

γ_w is the volumetric weight of liquid water (in N.m^{-3}), p_w is the pore pressure of liquid water. p_g is the pore pressure of the gas phase (made of air and vapor), and $\sigma(T)$ is the superficial energy of pore water (in $J.m^{-2}$). Combining equation 32 to the expression of the gradient of the hydraulic potential Φ_w (defined in equations 33 and 34), results in:

$$V_{wi} \;=\; -\frac{\Psi_R\left(\theta_w\right)}{\sigma(T_{ref})}\,\frac{d\sigma(T)}{dT}\,K_{wij}\,\nabla_j\left(T\right) - \frac{\sigma(T)}{\sigma(T_{ref})}\,\frac{d\Psi_R\left(\theta_w\right)}{d\theta_w}\,K_{wij}\,\nabla_j\left(\theta_w\right) - K_{wij}\,\nabla_j\left(z\right) \tag{36}$$

Introducing the definition of suction in equation 35, and combining the result to equation 36, finally gives the thermo-hydro-mechanical expression of the liquid water velocity:

$$V_{wi} \;=\; -D_{Twij}\,\nabla_j\left(T\right) \;+ D_{Pwij}\,\nabla_j\left(s\right) \;- K_{wij}\,\nabla_j\left(z\right) \tag{37}$$

in which:

$$\begin{cases} D_{Twij} \;=\; \frac{\Psi_R(\theta_w)}{\sigma(T_{ref})}\,\frac{d\sigma(T)}{dT}\,K_{wij} \\ \\ D_{Pwij} \;=\; \frac{1}{\gamma_w}\,\frac{\sigma(T)}{\sigma(T_{ref})}\,K_{wij} \end{cases} \tag{38}$$

4.1.2. Relative Permeabilities

The water permeability tensor is split as follows:

$$K_{wij} \;=\; k_T(T)\, k_r(S_w)\, K_{intij}\,(n, \Omega_{pq}) \tag{39}$$

The intrinsic permeability $K_{intij}\,(n, \Omega_{pq})$ is a second-order tensor, the coefficients of which are expressed in m.s^{-1}. It models the influence of the geometry of the porous network on the permeability of the REV to liquid water in saturated conditions. Both relative permeabilities $k_T(T)$ and $k_r(S_w)$ are scalar and non-dimensional, and characterize the liquid phase, independently of the solid matrix of the REV. It is recalled that S_w is the saturation degree of liquid water. As in the preceding models of unsaturated porous media developed by of Gatmiri [32], temperature is assumed to influence water viscosity $\mu_w(T)$ as follows:

$$k_T(T) \;=\; \frac{\mu_w(T)}{\mu_w(T_{ref})} \tag{40}$$

and the capillary relative permeability is written as:

$$k_r(S_w) = \left(\frac{S_w - S_{w,r}}{1 - S_{w,r}}\right)^3 \tag{41}$$

$S_{w,r}$ is the residual saturation degree, quantifying the remaining water menisci in the desaturated material. The water saturation degree is controlled by a state surface. The exponential influence of temperature on the saturation degree, formerly proposed in the works of Gatmiri [32, 34, 47], is kept unchanged. The hydraulic part is inspired from Van Genuchten retention curve [76]. Finally, the expression of the state surface chosen for the saturation degree in the THHMD model is the following (See Fig. 2):

$$\begin{cases} S_w \;=\; \left[(1 - S_{w,r})\;(1 \;+\; (\alpha_{VG}\, s)^{n_{VG}})^{-1+\frac{1}{n_{VG}}} \;+\; S_{w,r}\right] exp\,(d_s\,(T - T_0)) \quad if \quad s \geq 0 \\ S_w \;=\; 1 \quad if \quad s < 0 \end{cases} \tag{42}$$

α_{VG} and n_{VG} are Van Genuchten parameters. d_s quantifies the influence of temperature on the saturation degree.

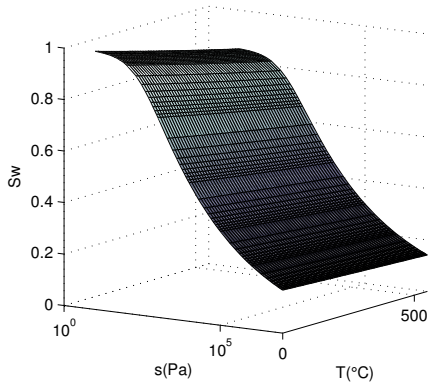

Figure 2: State Surface of the Saturation Degree. $T_0 = 20\,^oC$, $d_s = -3.10^{-4}\,^oC^{-1}$. The Van Genuchten parameters are typical of clays [76]: $\alpha_{VG} = 1.52.10^{-3}Pa^{-1}$, $n_{VG} = 1.17$.

4.1.3. Intrinsic Permeability

The intrinsic permeability $K_{intij}\left(n, \Omega_{pq}\right)$ is a skeleton property, and thus depends on the pore size distribution of the matrix. In undamaged states, it can be represented in the same way as for intact porous media. On the contrary, if the material is damaged, the formation of a fracture network influences the permeability of the matrix. Moreover, cracking orients the flow. That is the reason why $K_{intij}\left(n, \Omega_{pq}\right)$ is assumed to depend on total porosity n and damage Ω_{ij}. Cracks typical sizes exceed the typical sizes of the natural pores [55]. At the scale of the REV, the pores of the intact matrix form a homogeneous porous network, and each crack is connected to this natural porous network. As a result, even when damage is low, cracking implies a permeability increase. That is the reason why the intrinsic permeability of the damaged porous medium is written as the sum of intact and damaged components:

$$K_{intij}\left(n, \Omega_{pq}\right) \;=\; k_{1ij}\left(n^{rev}\right) \;+\; k_{2ij}\left(n^{frac}, \Omega_{pq}\right) \tag{43}$$

- $k_{1ij}\left(n^{rev}\right)$ is the permeability related to the reversibly deformed pores of the matrix. In the elastic domain, it is equal to the permeability which would be supported by an intact porous medium. Following the

approach of Gatmiri [32]:

$$k_{1ij}\left(n^{rev}\right) \,=\, k_{w_0}\, 10^{\alpha_w\, e^{rev}}\, \delta_{ij} \,=\, k_{w_0}\, 10^{\alpha_w\, e}\, \delta_{ij} \,=\, k_{1ij}\left(n\right) \tag{44}$$

k_{w_0} is the reference intrinsic permeability of the material when saturated (in m.s^{-1}). e^{rev} is the void ratio computed with the reversible components of volumetric strains. α_w is a non-dimensional material parameter.

- $k_{2ij}\left(n^{frac}, \Omega_{pq}\right)$ represents the additional permeability originated by fracturing. Cracks are assumed to be connected together by the intact (i.e. natural) porous network [56]. It is thus possible to assume that the flow of liquid water in the micro-cracks is equal to the flow which would occur in the corresponding equivalent cracks (considered connected). Moreover, assuming that cracks create preferential hydraulic flow paths does not contradict the absence of mechanical interaction between cracks (assumed in Section 2). It is important to note that healing is not accounted for in this preliminary permeability model.

The equivalent cracks defined in Section 2 are assumed to form a tubular network, in which the flow of liquid water is laminar. Following the approach of Shao's research team [72], the liquid flow generated by damage growth is thus be expressed by Poiseuille's cubic law for each equivalent crack. Using the same notations as in 3 and 4, the velocity of water in the I^{th} equivalent crack may be written as [72]:

$$V_{wi}^{\,I} \,=\, -k_T(T)\, k_r(S_w)\, \frac{1}{12\, \mu_w\left(T_{ref}\right)}\, \left(e^I\right)^2\, \left(\delta_{ij} - n_i^I\, n_j^I\right)\, \nabla_j\left(\gamma_w\left(\Psi_w \,+\, z\right)\right) \tag{45}$$

Assuming that the equivalent cracks are penny-shaped and that the REV is a cube of side b, the velocity of the liquid in the fracture network may be averaged as follows:

$$V_w^{frac}{}_i \,=\, \frac{1}{b^3} \sum_{I=1}^{3} \left[V_{wi}^{\,I}\, \pi\, \left(l^I\right)^2\, e^I\right] \tag{46}$$

The introduction of 45 in 46 results in:

$$V_w^{frac}{}_i \,=\, -k_T(T)\, k_r(S_w)\, \frac{\gamma_w}{12\, \mu_w\left(T_{ref}\right)} \frac{\pi}{b^3}\, \left[\sum_{I=1}^{3} \left(e^I\right)^3\, \left(l^I\right)^2\, \left(\delta_{ij} - n_i^I\, n_j^I\right)\right]\, \nabla_j\left(\Psi_w \,+\, z\right) \tag{47}$$

The definition of the damaged intrinsic permeability imposes:

$$V_w^{frac}{}_i \;=\; -k_T(T)\, k_r(S_w)\, k_{2ij}\left(n^{frac}, \Omega_{pq}\right)\, \nabla_j\left(\Psi_w \;+\; z\right) \tag{48}$$

By identification, considering that the equivalent cracks are penny-shaped and using the dilatancy law stated in equation 4:

$$k_{2ij}\left(n^{frac}, \Omega_{pq}\right) \;=\; \frac{\pi^{-2/3}\,\gamma_w}{12\,\mu_w\left(T_{ref}\right)}\,\chi^{4/3}\,b^2\,\sum_{I=1}^{3}\left(d^I\right)^{5/3}\,\left(\delta_{ij} - n_i^I\, n_j^I\right) \tag{49}$$

In formula 49, b plays the role of an internal length parameter, which is specific to the liquid flow problem. It may be computed if the value of the damaged intrinsic permeability is known for a given rate of damage. In the following numerical examples, a maximal crack-related permeability k_{wdg}^{max} is introduced in the input parameters in order to scale the global damaged permeability for an isotropic damage state of $\Omega_{ij} = 0.95\delta_{ij}$.

4.2. Vapor Flow

4.2.1. Vapor Flow in the Intact Porous Medium

The flow velocity of vapor is defined as:

$$V_{vap_i} \;=\; \frac{1}{\rho_{vap}}\, Q_{\,vap_i} \tag{50}$$

According to the model of Philip and de Vries [64], the vapor flow $Q_{\,vap_i}$ may be expressed as:

$$Q_{\,vap_i} \;=\; -1.024\, D_0\, n(1 - S_w)\, \nabla_i\left(\rho_{vap}\right) \tag{51}$$

D_0 is the molecular diffusivity of vapor in air (in $m^2.s^{-1}$). Vapor density ρ_{vap} (in kg.m^{-3}) is assumed to depend on water content θ_w and on temperature, as follows:

$$\rho_{vap} \;=\; h\left(\theta_w, T\right)\, \rho_{vap}^0\left(T\right) \tag{52}$$

ρ_{vap}^0 is the density of vapor in saturated conditions, and is assumed to depend on temperature only. $h\left(\theta_w, T\right)$ is the relative humidity of the medium. It is non-dimensional and may be expressed as [64]:

$$h\left(\theta_w, T\right) \;=\; exp\left(\frac{\Psi_w\, g}{R_{vap}\, T}\right) \tag{53}$$

R_{vap} is the mass density of the constant of perfect gases for vapor. Ψ_w is the capillary potential of water (equation 34). g is the gravity acceleration (in m.s^{-2}) and T is temperature (in ^oC). Philip and de Vries [64] showed that the variation of relative humidity with water content dominated the variation of relative humidity with temperature, so that the latter could be neglected. Therefore, using equations 52, 53 and 34:

$$\nabla_i(\rho_{vap}) = h(\theta_w,T)\,\frac{d\rho^0_{vap}(T)}{dT}\,\nabla_i(T) + h(\theta_w,T)\,\rho^0_{vap}(T)\,\frac{g}{R_{vap}\,T}\,\frac{\partial\Psi_w(\theta_w,T)}{\partial\theta_w}\,\nabla_i(\theta_w) \tag{54}$$

Heat exchanges between the solid matrix and the pore fluids dominate heat transfers at the scale of the REV [30, 34]. This can be modeled by introducing the ratio of the gradient of temperature at the micro-scale to the gradient of temperature at the macro-scale: $(\nabla_k(T))_a/\nabla_k(T)$. Thus considering that the volumetric fraction of material which is active in heat transfers is the total porosity n instead of the gas porosity $n(1-S_w)$ [26, 66], and combining equations 50, 51 and 54, the expression of the vapor flow velocity results in:

$$\begin{array}{l} V_{vap_i} = -\frac{1.024\,D_0\,n}{\rho_{vap}}\left[h(\theta_w,T)\,\frac{d\rho^0_{vap}(T)}{dT}\,\frac{(\nabla_k(T))_a}{\nabla_k(T)}\,\nabla_i(T)\right] \\ -\frac{1.024\,D_0\,n}{\rho_{vap}}\left[h(\theta_w,T)\,\rho^0_{vap}(T)\,\frac{g}{R_{vap}\,T}\,\frac{\partial\Psi_w(\theta_w,T)}{\partial\theta_w}\,\nabla_i(\theta_w)\right] \end{array} \tag{55}$$

The determination of $(\nabla_k(T))_a/\nabla_k(T)$ is explained in detail in the works of Ewen and Thomas [26]. After using definition 34, the final expression of the vapor flow velocity may be written as:

$$V^*_{vap_i} = \frac{\rho_{vap}}{\rho_w}\,V_{vap_i} = -D_{T_{vap}}\,\nabla_i(T) + D_{P_{vap}}\,\nabla_i(s) \tag{56}$$

in which:

$$\left\{\begin{array}{l} D_{T_{vap}} = \frac{1}{\rho_w}\,D_{int,\,vap}\,\frac{(\nabla(T))_a}{\nabla(T)}\,h(\theta_w,T)\,\frac{d\rho^0_{vap}(T)}{dT} \\ \\ D_{P_{vap}} = \frac{1}{\rho_w}\,D_{int,\,vap}\,\rho_{vap}(\theta_w,T)\,\frac{g}{R_{vap}\,T}\,\frac{1}{\gamma_w}\,\frac{\sigma(T)}{\sigma\left(T_{ref}\right)} \\ \\ D_{int,\,vap} = 1.024\,D_0\,n \end{array}\right. \tag{57}$$

4.2.2. Extension of the Vapor Flow Model to Damaged Materials

As in the preceding flow model for liquid water, it is assumed that cracking

accelerates vapor transfers in such a way that the flow formulas used for the intact porous medium become invalid. The vapor intrinsic conductivity $D_{int,\,vap}$ is split into two parts:

(i) a conductivity relative to the pores of the matrix, taken in their reversible domain of deformation: $D_{int,\,vap_1}\left(n^{rev}, s, T, \Omega_{pq}\right)$;

(ii) a conductivity generated by the creation of a fractures network: $D_{int,\,vap_2}\left(n^{frac}, \Omega_{pq}\right)$.

In order to extend the computation of vapor flow (equations 56 and 57) to damaged states, the vapor intrinsic conductivity is thus changed into:

$$D_{int,\,vap} \;=\; D_{int,\,vap_1}\left(n^{rev}, s, T, \Omega_{pq}\right) \;+\; D_{int,\,vap_2}\left(n^{frac}, \Omega_{pq}\right) \qquad (58)$$

in which the conductivity relative to the pores $D_{int,\,vap_1}\left(n^{rev}, s, T, \Omega_{pq}\right)$ is expressed in the same manner as for the intact material (equation 57), but for the reversible domain of deformations only:

$$D_{int,\,vap_1}\left(n^{rev}, s, T, \Omega_{pq}\right) \;=\; 1.024\, D_0\, n^{rev} \qquad (59)$$

It is assumed that vapor goes much faster than liquid water, and that consequently, the fracture network hardly affects the orientation of vapor flow. That is the reason why the damaged component of the vapor intrinsic conductivity is expressed as a function of the mean damaged intrinsic conductivity of liquid water $k_{2ij}\left(n^{frac}, \Omega_{pq}\right)$:

$$D_{int,\,vap_2}\left(n^{frac}, \Omega_{pq}\right) \;=\; \frac{b^*}{3}\,\delta_{ij}\,k^*_{2ji}\left(n^{frac}, \Omega_{pq}\right) \qquad (60)$$

in which the damaged intrinsic conductivity of liquid water is expressed with the vapor transfer internal length b^* (equation 49):

$$k^*_{2ij}\left(n^{frac}, \mathbf{\Omega}\right) \;=\; \frac{\pi^{-2/3}\,\gamma_w}{12\,\mu_w\left(T_{ref}\right)}\,\chi^{4/3}\;\left(b^*\right)^2\,\sum_{I=1}^{3}\left(d^I\right)^{5/3}\;\left(\delta_{ij} - n^I_i\,n^I_j\right) \qquad (61)$$

As for the liquid water flow model, the internal length parameter b^* may be evaluated if the damaged intrinsic conductivity of vapor is known for a given state of damage. In the following numerical examples, a maximal crack-related vapor diffusivity D^{max}_{dg} is introduced in the input parameters in order to scale the global damaged vapor conductivity for an isotropic damage state of $\Omega_{ij} = 0.95\delta_{ij}$.

4.3. Air Flow

Air flow, like liquid water and vapor flows, is assumed to obey an extended Darcy law. The introduction of a gradient of air pore pressure induces a dependence of air flow to the gradient of temperature:

$$\begin{array}{l} V_{ai} \,=\, -K_{aij}\,\nabla_j\left(\frac{p_a}{\gamma_a} \,+\, z\right) \\ \,=\, -\frac{1}{\gamma_a}\,\frac{\partial p_a(\mathbf{x},T(\mathbf{x}))}{\partial T(\mathbf{x})}\,K_{aij}\,\nabla_j\left(T(\mathbf{x})\right) \,-\, K_{aij}\,\nabla_j\left(\frac{p_a}{\gamma_a}\right) \,-\, K_{aij}\,\nabla_j\left(z\right) \end{array} \tag{62}$$

Due to its high velocity relatively to liquid water and vapor flows, air transfer is assumed to be poorly influenced by the formation of cracks. That is the reason why no specific fracture conductivity is introduced. The isotropic model of air permeability used by Gatmiri [30, 31, 32, 33] is kept unchanged:

$$K_{aij} \,=\, c_a\,\frac{\gamma_a}{\mu_a}\,\left[e(1-S_w)\right]^{\alpha_a}\,\delta_{ij} \tag{63}$$

γ_a (in N.m^{-3}) and μ_a (in N.S.m^{-2}) are the volumetric weight and dynamic viscosity of air respectively. c_a and α_a are material parameters. e is the total void ratio, and thus depends on damage. The influence of cracking on air flow is also taken into account through the dependence on the saturation degree, which is related to the permeability changes induced by cracking. Damage is thus accounted for by volumetric entities. As a consequence, air transfers are homogenized at the scale of the degraded REV, and damage cannot orient air flow.

4.4. Heat Flow

As in Gatmiri's preceding models [30, 31, 32], heat transfer is assumed to be governed by diffusion, convection and evaporation. Convection and evaporation are pure fluid phenomena. Only the diffusive part of heat transfer is likely to be influenced by the degradation of the solid matrix. Heat flow is assumed to be governed by the same equation as in the intact state:

$$\begin{array}{l} Q_{Ti} \,=\, -\,\lambda_T\,\nabla_i\left(T\right) \,+\, h_{fg}\,\left(\rho_w\,V^*_{vap_i} \,+\, \rho_{vap}\,V_{ai}\right) \\ +\,\left[\rho_w\,C_{Pw}\,V_{wi} \,+\, \rho_w\,C_{Pvap}\,V^*_{vap_i} \,+\, \rho_a\,C_{Pa}\,V_{ai}\right]\,(T \,-\, T_0) \end{array} \tag{64}$$

(i) $-\lambda_T\,\nabla_i\left(T\right)$ is the diffusive transfer term, λ_T being Fourier's thermal conductivity. Assuming that the constituents of the REV are set in parallel, λ_T may be computed as [27]:

$$\lambda_T \,=\, (1-n)\,\lambda_s \,+\, n\,S_w\,\lambda_w \,+\, n\,(1-S_w)\,\lambda_{vap} \tag{65}$$

in which λ_s, λ_w and λ_{vap} are the thermal conductivities of the solid skeleton, liquid water and vapor respectively. As for air flow, cracking influences the diffusive transfer isotropically, through an increase of porosity.

(ii) $h_{fg}\left(\rho_w V^*_{vap_i} + \rho_{vap} V_{ai}\right)$ quantifies the influence of evaporation on heat transfer. In the usual temperature and pressure conditions, the evaporation latent heat is $h_{fg} = 2,4 * 10^6\, J.kg^{-1}$.

(iii) $\left[\rho_w C_{Pw} V_{wi} + \rho_w C_{Pvap} V^*_{vap_i} + \rho_a C_{Pa} V_{ai}\right](T - T_0)$ describes convective transport. C_{Pw}, C_{Pvap} and C_{Pa} are the specific heats of liquid water, vapor and air respectively (in $J.kg^{-1}.^oC^{-1}$)

5. BALANCE EQUATIONS

In the following, vectors and tensors are represented in bold characters to avoid heavy indice notations.

5.1. Balance Equation of the Solid Skeleton

The balance equation for the solid skeleton writes:

$$\nabla \cdot \sigma + \mathbf{F} = \mathbf{0} \tag{66}$$

in which σ is Cauchy's total stress tensor, and $\mathbf{F}$ is a distant external volumetric force exerted on the system (used to account for gravitational effects).

5.2. Moisture Mass Conservation Equation

The mass conservation equation of moisture writes:

$$\frac{\partial \rho_m}{\partial t} + \nabla \cdot \left(\rho_w \left(\mathbf{V_w} + \mathbf{V^*_{vap}}\right)\right) = 0 \tag{67}$$

Assuming that air and vapor form a perfect gas mixture, and that both constituents occupy the same pore spaces:

$$\rho_m = nS_w\rho_w + n(1 - S_w)\rho_{vap} \tag{68}$$

The determination of the global governing equation of moisture requires the expressions of the partial time derivatives of n, S_w, ρ_w and ρ_{vap}. The computations are provided in the appendices.

5.3. Air Mass Conservation Equation

The mass conservation equation of air is:

$$\frac{\partial}{\partial t}\left(n\,\rho_a\,(1-S_w+HS_w)\right)+\nabla\cdot(\rho_a\,\mathbf{V_a})+\nabla\cdot(\rho_a\,H\,\mathbf{V_w})-\nabla\cdot(\rho_w\,\mathbf{V_{vap}}^*)\;=\;0 \tag{69}$$

The presence of Henry's constant H in equation 69 indicates that there is some dissolved air in liquid water. In usual pressure and temperature conditions, $H = 0.02$. The global governing equation for air requires the determination of $\frac{\partial \rho_a}{\partial t}$. Air is considered as a perfect gas of constant R_a:

$$\begin{cases} \frac{\partial \rho_a}{\partial t} \;=\; \alpha_P\,\frac{\partial p_a}{\partial t}\;+\alpha_T\,\frac{\partial T}{\partial t} \\ \\ \alpha_P \;=\; \frac{1}{R_a\,T}, \quad \alpha_T \;=\; -\frac{p_a+p_{atm}}{R_a\,(T+273.15)^2}, \quad R_a = 9.448.10^2\;J.K^{-1}.kg^{-1} \end{cases} \tag{70}$$

5.4. Energy Conservation Equation

The energy conservation equation writes:

$$\frac{\partial \phi}{\partial t}\;+\;\nabla\cdot\mathbf{Q_T}\;=\;0 \tag{71}$$

in which the thermal energy received by the REV, considered as an open system, writes:

$$\phi\;=\;C_T\,(T-T_0)\;+n(1-S_w)\rho_{vap}\,h_{fg} \tag{72}$$

The REV's specific heat may be computed as if all the constituents were put in parallel:

$$C_T\;=\;(1-n)\rho_s\,C_{Ps}\;+\;nS_w\rho_w\,C_{Pw}\;+n(1-S_w)\rho_{vap}\,C_{Pvap}\;+n(1-S_w)\rho_a\,C_{Pa} \tag{73}$$

The solid phase is assumed to be incompressible ($\frac{\partial \rho_s}{\partial t} = 0$). Equation 70, and the computations given in the appendices (equations 81, 82, 83 and 84) may then be used to determine the complete heat governing equation.

6. NUMERICAL STUDIES

A specific algorithm has been written in order to implement the THHMD model in Θ-Stock Finite Element code [32], which has been used to perform the simulations presented in this article.

Table 1: Main Material Parameters used to Simulate the Triaxial Compression Test on Sandstone.

E (Pa)	ν	e_0	g_M (Pa)	C_0 (Pa)	C_1 (Pa)
$1.17 * 10^{10}$	0.2	0.2658	$-3.2 * 10^7$	$2 * 10^4$	$2.7 * 10^5$

6.1. Mechanical Laboratory Tests (Numerical Validation)

Mechanical experimental tests performed on granite, clay rock and sandstone have been simulated. The numerical results have been compared to the experimental measurements reported in reference articles. The mechanical aspects of the THHMD model have been validated on:

- triaxial compression tests, lateral extension tests and proportional compression tests performed on dry geomaterials [1, 5],
- triaxial compression tests performed on saturated sandstone, in drained and undrained conditions [1, 5].

In Figure 3, the results obtained on a triaxial compression test performed on dry sandstone are compared to experimental data provided by Dragon et al. [24]. The main material parameters required in Θ-Stock to run the simulations are reported in Tab. 1. Numerical strain predictions match the experimental measurements (Fig. 3.a). The axial compression generates tensile mechanical strains in both lateral directions, so that $\Omega_{rr} = \Omega_{\theta\theta} \neq 0$, $\Omega_{zz} = 0$. As expected, damage grows with the deviatoric stress applied to the sample during the compression test (Fig. 3.b).

6.2. Influence of Thermal Cracking on Damage Development (Parametric Study)

6.2.1. Problem Description: A One-Dimensional Thermo-Mechanical Model for Nuclear Waste Repositories

This first numerical example is a simplified study of the problem of nuclear waste storage. It is based on former numerical works published by Carter and Booker [13]. The radioactive package is assumed to be stored in a deep, cylindrical, well-bore, of radius R. The initial temperature of the host rock

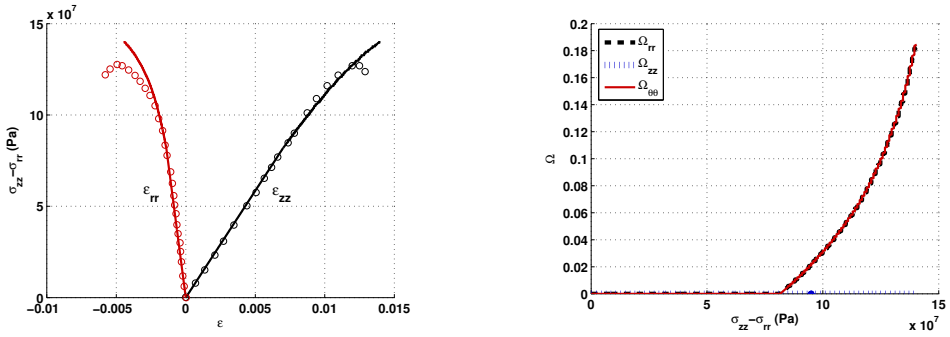

a. b.

Figure 3: Triaxial compression test performed on dry sandstone for a confining pressure of 15 MPa. a. Stress/strain curves (presented with the soil mechanics sign convention). Dots: experimental data [24]. Solid lines: Θ-Stock numerical results. b. Evolution of the components of the damage tensor.

is 0^oC. The temperature imposed by waste is assumed to increase linearly during two years, and then to decrease exponentially, as follows:

$$\begin{cases} \widetilde{T}(t) = 25\,t \quad if \quad t \leq 2\,years \\ \widetilde{T}(t) = 50\,exp\,(0.0288\,-0.0144\,t) \quad if \quad t \geq 2\,years \end{cases} \tag{74}$$

The FEM program of Carter and Booker only depends on thermal and mechanical degrees of freedom. The simulations may be reproduced in Θ-Stock by assuming that the rock mass is made of a porous rock which is not subjected to any fluid pore pressure. Physically, the geological barrier is thus assumed to be almost dry. In Θ-Stock, the pore pressure degrees of freedom are thus neutralized. The cylindrical geometry and the diffusive character of the imposed loading make it possible to perform simulations in an axis-symmetric configuration. The adopted mesh and boundary conditions are shown in Fig. 4. The Young modulus and Poisson ratio of the host rock are provided by Carter and Booker [13]. The specific weight is fixed to a usual value: $\gamma_s = 2.65 * 10^4\,N.m^{-3}$. The initial void ratio of the material is assumed to be in the range of values observed for granite [45]. In the absence of damage data in the reference article, the damage-associated rates C_0 and C_1 have been fixed to the values determined by Halm and Dragon for granite [43]. The first simulations are run in the reversible domain, so that $g_M = g_S = g_T = 0$. A standard value is used for the rock's specific heat. Carter and Booker fix the value of a non-dimensional conductivity parameter

κ so that:

$$\kappa \;=\; \frac{\lambda_s}{\rho_s\, C_{Ps}} \;=\; 0.02\, m^2.year^{-1} \tag{75}$$

This imposes a very small value for the thermal conductivity λ_s (Tab. 2). The incremental stress/strain relationship used by Carter and Booker is based on a classical thermo-elastic behavior law:

$$d\sigma_{ij} \;=\; D_{eijkl}\, d\epsilon^e_{lk} \;-\; \frac{E\,\alpha}{(1-2\nu)}\delta_{ij}\, dT \tag{76}$$

In the THHMD model, the elastic stress/strain relationship writes:

$$d\sigma"_{ij} \;=\; D_{eijkl}\, d\epsilon^e_{Mlk} \;=\; D_{eijkl}\, d\epsilon^e_{lk} - \frac{1}{3} D_{eijkl}\, \delta_{lk}\, d\epsilon^e_{Sv} - \frac{1}{3} D_{eijkl}\, \delta_{lk}\, d\epsilon^e_{Tv} \tag{77}$$

In an intact material:

$$d\sigma"_{ij} \;=\; D_{eijkl}\, d\epsilon^e_{lk} \;-\; \frac{1}{3\,\beta^0_s} D_{eijkl}\, \delta_{lk}\, ds \;-\; \frac{\alpha^*_0}{3}\, D_{eijkl}\, \delta_{lk}\, dT \tag{78}$$

In this example, there is no pore pressure degree of freedom, so that:

$$d\sigma_{ij} \;=\; D_{eijkl}\, d\epsilon^e_{lk} \;-\; \frac{\alpha^*_0}{3} D_{eijkl}\, \delta_{lk}\, dT \tag{79}$$

The combination of equations 76 and 79 provides the value of the thermal expansion coefficient that should be used in Θ-Stock. The coefficient obtained is adapted to be used in a 2D numerical computation frame (in which one of the three components of 3D strains is zero) [1]. Note that the sign of α^*_0 is opposite to the sign of the coefficient used by Carter and Booker, because Carter and Booker use the Continuum Mechanics Convention sign (in which compressions are counted negatively), whereas in Θ-Stock, the Soil Mechanics sign convention (in which compressions are assumed to be positive) is adopted. The thermo-mechanical parameters used in this simulation are reported in Tab. 2.

6.2.2. Verification of the Results in the Reversible Domain (No Damage Development)

The reference article by Carter and Booker [13] focuses on elastic problems only. The first step of this study consists in comparing the results obtained

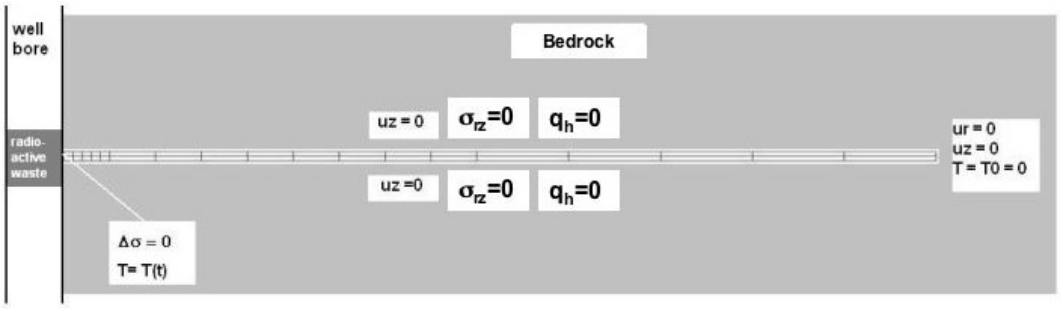

Figure 4: Mesh and Boundary Conditions for the Thermo-Mechanical Problem of Nuclear Waste Storage [13].

Table 2: Thermo-Mechanical Material Parameters used in the Simplified Repository Model [13].

E (Pa)	ν	e_0	C_0 (Pa)	C_1 (Pa)
$8 * 10^{10}$	0.3	0.00351	$1.1 * 10^5$	$2.2 * 10^6$
C_{Ps} $(J.kg^{-1}.{}^oC^{-1})$	λ_s $(W.m^{-1}.{}^oC^{-1})$	α_0^* $({}^oC^{-1})$		
800	$1.37 * 10^{-3}$	$-2 * 10^{-5}$		

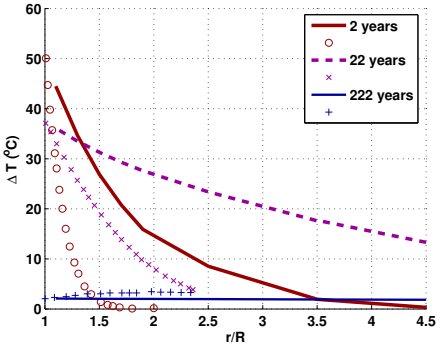

Figure 5: Temperature evolution in the bedrock, in the vicinity of nuclear waste. Dots: reference results from [13]. Solid lines: numerical results obtained with Θ-Stock in the elastic domain of the THHMD model.

with Θ-Stock with the reference results provided in the article, in order to check the ability of the program to solve coupled problems. Figures 5 and 6 show that the match is good in the steady state (after 222 years of storage). The equilibrium state computed in stress and temperature is thus the same with both programs, which justifies the choice of the thermal expansion coefficient explained in the previous paragraph. In transient stages, the trends and orders of magnitudes of the results obtained with Θ-Stock are physically consistent, but do not match the reference results of Carter and Booker. In fact the kinetics are not respected: the curves obtained with Θ-Stock after 2 years of heating are closer to the curves obtained by Carter and Booker after 22 years of storage than after 2 years of storage. It seems that the thermo-mechanical equilibrium is reached faster with Θ-Stock.

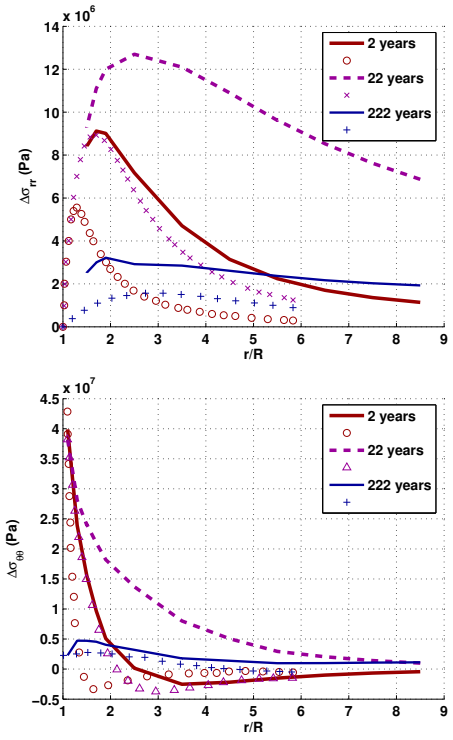

a. b.

Figure 6: Stress evolution in the bedrock, in the vicinity of nuclear waste. a. Radial stress variations. b. Orthoradial stress variations. Dots: reference results from [13]. Solid lines: numerical results obtained with Θ-Stock in the elastic domain of the THHMD model.

6.2.3. Parametric Study of Damage

In the following, it is assumed that the rock mass modeled in the thermo-mechanical storage problem described above may be damaged (i.e. the state variables may evolve out of the reversible domain). Due to the type of loading applied in the simulation, it is expected that thermal dilatation be the dominating source of damage ($\epsilon_{Tv}^{+} \neq 0$). In order to enhance the potential effects of thermal cracking in the following parametric studies, g_T will be the only resistance to cracking which will be set to a non-zero value. g_T stems from one of the pioneering aspects of the THHMD model. That is the reason why there is no reference value in the literature. In order to work in a reasonable order of magnitude, values close to the mechanical resistance to cracking (g_M) will be tested. In the following, g_M^{ref} stands for the mechanical resistance to cracking determined for granite by Halm and Dragon [43], which amounts to $-3.3 * 10^8\, Pa$ (the minus sign comes from the soil mechanics convention). After numerous series of simulations, the most relevant results turned out to be obtained for $4 * g_M^{ref} \leq g_T \leq 4.3 * g_M^{ref}$.

Provided that g_T is the only non-zero resistance to cracking, damage can only increase with thermal dilatation ϵ_{Tv}^{+} (equations 29 and 30). Thermal strains are assumed to be isotropic (equation 6), so that the damage driving force $Y_{d1\,ij}^{+}$ is isotropic: $Y_{d1\,ij}^{+} = g_T\, \frac{1}{3}\epsilon_{Tv}^{+}\, \delta_{ij}$. Potential damage is thus isotropic (equation 31). In the simulations, isotropic damage is observed, which meets the model requirements (this constitutes a verification of the model implementation in Θ-Stock). In Fig. 7, only radial damage is represented. g_T varies in a too slight interval to generate a huge difference in the peak value of damage. The maximal damage is 2% higher with $g_T = 4.3 * g_M^{ref}$ than with $g_T = 4 * g_M^{ref}$ (Fig. 7.b,d,f). As expected, damage reaches a maximum value in the zone which is in contact with the heating source. The peak value is obtained after two years, which corresponds to the end of the linear increase of waste temperature. When the heating power then decreases, the close neighbourhood of the well-bore is relaxed, but heat continues to propagate in the bedrock. That is the reason why the damaged zone continues to spread, especially during the first twenty years of relaxation (Fig. 7.a,c,e). The more damage grows, the more irreversible strains develop, as can be observed in the vicinity of the nuclear waste package (Fig. 8). The comparison of Fig. 8.b,d and Fig. 8.f,h indicates that irreversible thermal

strains (ϵ_{Tv}^{irr}) mainly impact the global radial deformation of the rock mass (ϵ_{rr}). Granite is a very rigid material. The huge value of the Young modulus explains why the variation of thermal strains with g_T is much less than the global variations of all types of deformations with heating power. As expected, in the vicinity of the heating source, the bedrock encounters tensile strains (negative deformations with the soil mechanics convention). In the zone of contact with waste, tensile strains increase as long as the heating power increases. After two years, i.e. during the relaxation period, strains stabilize. The observation of damage evolution in space shows that strains continue to evolve during the relaxation period, but at some distance of the well (Fig. 7.a,c,e).

6.3. Effect of Damage on the Degree of Saturation (Parametric Study)

6.3.1. Problem: A Laboratory Heating Test on Deformable Unsaturated Compacted Clay

In the following, the heating test performed by Villar et al. [78] in a tank filled with unsaturated compacted clay is reproduced numerically. Contrary to the preceding numerical study, the problem is fully coupled, and the simulation requires the use of all degrees of freedom (i.e. displacements, pore pressures and temperature). The tank is 14.6cm deep and 15cm wide. It is assumed to be long enough to enable a study in plane strain. The heating source is placed at the center and at the top of the tank. A 100^oC temperature is thus applied during two hours. The initial temperature of the soil is 20^oC. The external boundaries of the tank are assumed impervious and are continuously showered with water at 28^oC. The corresponding boundary conditions adopted in the numerical study are shown in Fig. 9. The void ratio and the saturation degree of the compacted clay are initialized at the values reported by Villar et al: 0.71 and 0.5 respectively. The reference article does not provide all the required material parameters. In the following, it is assumed that the mechanical behavior of the studied compacted clay is similar to the one of the clay stone studied by Homand et al. [45] and Chiarelli and Shao [15]. This assumption enables to work with a consistent set of damage and mechanical parameters (E, ν, C_0 and C_1 in elasticity, and then g_M for non-elastic cases). Thermal parameters are assigned standard values. Capillary parameters are fit in order to reproduce the retention and permeability properties used by Jenab [47] in the simulations she did on the same heating experiment. The choice of material parameters is explained

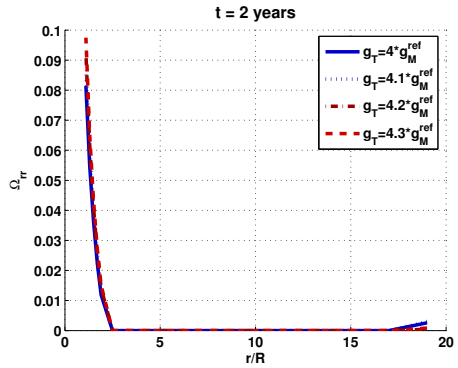
t = 2 years
$g_T=4*g_M^{ref}$
$g_T=4.1*g_M^{ref}$
$g_T=4.2*g_M^{ref}$
$g_T=4.3*g_M^{ref}$
Ω_{rr}
r/R

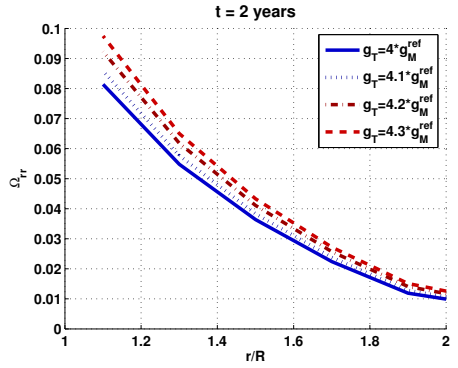
t = 2 years
$g_T=4*g_M^{ref}$
$g_T=4.1*g_M^{ref}$
$g_T=4.2*g_M^{ref}$
$g_T=4.3*g_M^{ref}$
Ω_{rr}
r/R

a. b.

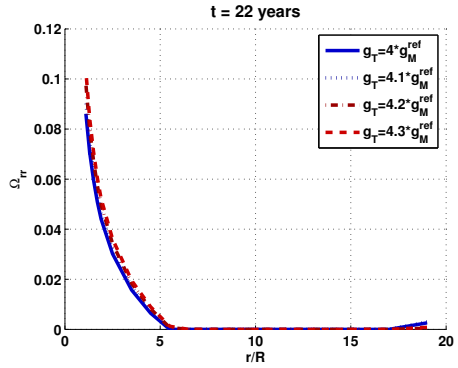
t = 22 years
$g_T=4*g_M^{ref}$
$g_T=4.1*g_M^{ref}$
$g_T=4.2*g_M^{ref}$
$g_T=4.3*g_M^{ref}$
Ω_{rr}
r/R

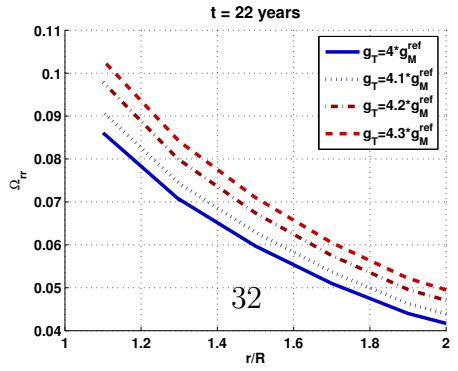
t = 22 years
$g_T=4*g_M^{ref}$
$g_T=4.1*g_M^{ref}$
$g_T=4.2*g_M^{ref}$
$g_T=4.3*g_M^{ref}$
Ω_{rr}
r/R

c. d.

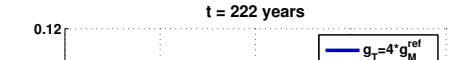
t = 222 years
$g_T=4*g_M^{ref}$

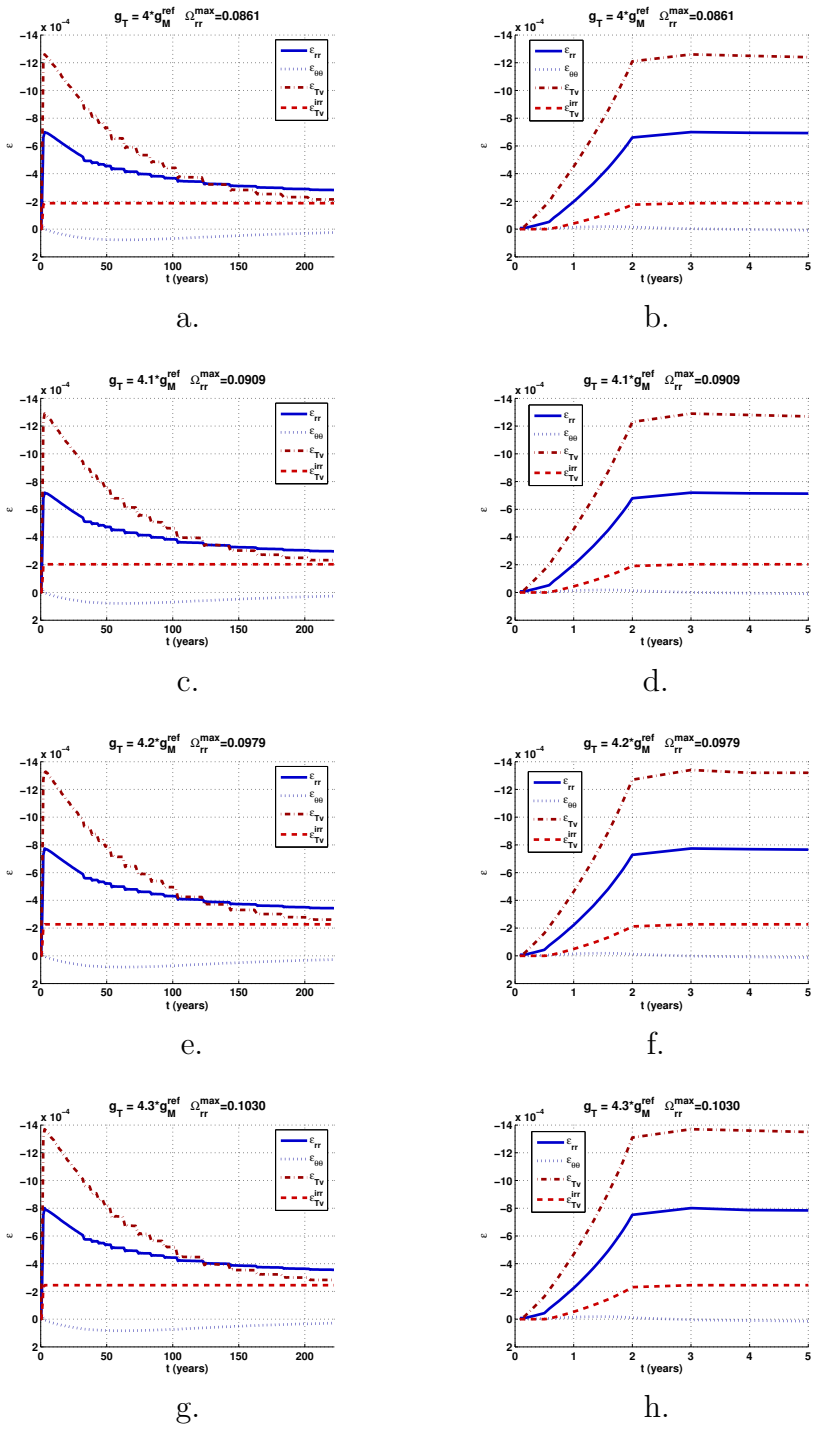

Figure 8: Axis-symmetric Study of the Thermo-Mechanical Brittle Behavior of a Granite Rock Mass. Time Evolution of Strains, Computed on a Finite Element next to Nuclear Waste. $g_T = 4 * g_M^{ref}$ (a,b), $g_T = 4.1 * g_M^{ref}$ (c,d), $g_T = 4.2 * g_M^{ref}$ (e,f) et $g_T = 4.3 * g_M^{ref}$ (g,h).

Table 3: Material Parameters Used to Model Elastic Compacted Clay in the Experiment of Villar et al. [78].

E (Pa)	ν	C_0 (Pa)	C_1 (Pa)	β_s^0 (Pa)	β_T^0 (Pa)
$1.22 * 10^{10}$	0.16	$2.3 * 10^{-4}$	$5.2 * 10^{-3}$	$5.98 * 10^{8}$	$5.98 * 10^{10}$
k_{w0} $(m.s^{-1})$	α_w	$S_{w,r}$	α_{VG} (Pa^{-1})	n_{VG}	d_s $(^oC^{-1})$
$1.2 * 10^{-5}$	0	0	$5 * 10^{-4}$	2.3	-10^{-5}
χ	k_{wdg}^{max} $(m.s^{-1})$	D_{dg}^{max} $(m^2.s^{-1})$	c_a (m^2)	α_a	
0.005	10^{-9}	10^{-4}	$3 * 10^{-12}$	4	
α_0^*	C_{Ps}	C_{Pw}	C_{Pvap}	C_{Pa}	
$(^oC^{-1})$	$(W.m^{-1}.^oC^{-1})$	$(W.m^{-1}.^oC^{-1})$	$(W.m^{-1}.^oC^{-1})$	$(W.m^{-1}.^oC^{-1})$	
$-7.5 * 10^{-4}$	837	4184	1900	1000	
λ_s	λ_w	λ_a	h_{fg}		
$(W.m^{-1}.^oC^{-1})$	$(W.m^{-1}.^oC^{-1})$	$(W.m^{-1}.^oC^{-1})$	$(J.kg^{-1})$		
1.05	0.6	0.0258	$2.5 * 10^{6}$		

in detail in [1]. The main input parameters used to solve the problem in elasticity are reported in Tab. 3.

6.3.2. Verification of the Results in the Reversible Domain (No Damage Development)

As in the previous thermo-mechanical study of waste storage, a first simulation is run in the absence of damage. This is aimed at verifying the implementation of the model and to test the algorithm programmed in Θ-Stock on complex, coupled problems. The temperature and degree of saturation after two hours of heating are represented in Fig. 10. The results are confronted to punctual experimental measurements. The comparison shows that the trends are well-reproduced: after two hours of heating, temperature is much higher than in the initial configuration in the vicinity of the source, and decreases as the distance to the source increases (Fig. 10.a). This results in evaporation near the source, with a migration of vapor away from the source. The degree of saturation becomes lower close to the source, and gets higher as the distance to the source increases (Fig. 10.b). In this particular numerical study, the temperature distribution after two hours of heating is more homogeneous than in the experiment, which means that what is predicted in the simulation is closer to the steady state than what is measured in the laboratory. In the experiment, condensation phenomena are observed near the

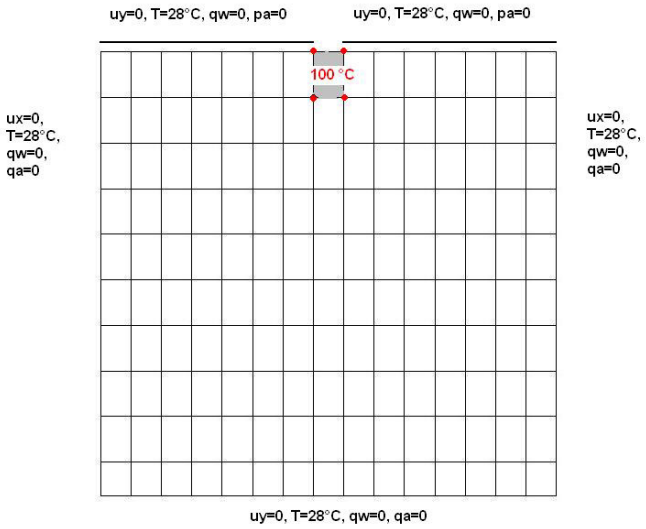

Figure 9: Boundary Conditions Adopted to Simulate Villar's Experiment [78].

tank walls ($S_w > S_{w0}$), whereas in the simulation, it seems that condensed vapor has already moved back to the source.

6.3.3. Parametric Study of Damage

In the following, the influence of the thermal resistance to cracking is investigated by varying the value of g_T parameter. The material parameters are kept the same as in the previous elastic configuration (Tab. 3), except g_T, $K^{max}_{w,\,dg}$ and $D^{max}_{vap,\,dg}$. These two latter parameters play the role of internal lengths (equations 49 and 61). Their values have no importance in the reversible domain, but have a strong influence on flows in a damaged material. In order to enhance the influence of cracking on conductivities, the former values of $K^{max}_{w,\,dg}$ and $D^{max}_{vap,\,dg}$ (Tab. 3) have been increased in the parametric study of damage:

$$K^{max}_{w,\,dg} \;=\; 100\,k_{w0} \;=\; 1.2\,10^{-3}\,m.s^{-1}, \quad D^{max}_{vap,\,dg} \;=\; 1.2\,10^{-1}\,m^2.s^{-1} \qquad (80)$$

As in the preceding thermo-mechanical study of nuclear waste storage, g_T has been varied in a range of values rather close to the available reference value of g_M for the material under investigation. In the simulation of Villar experiment, it has been assumed that the mechanical properties of the geomaterial

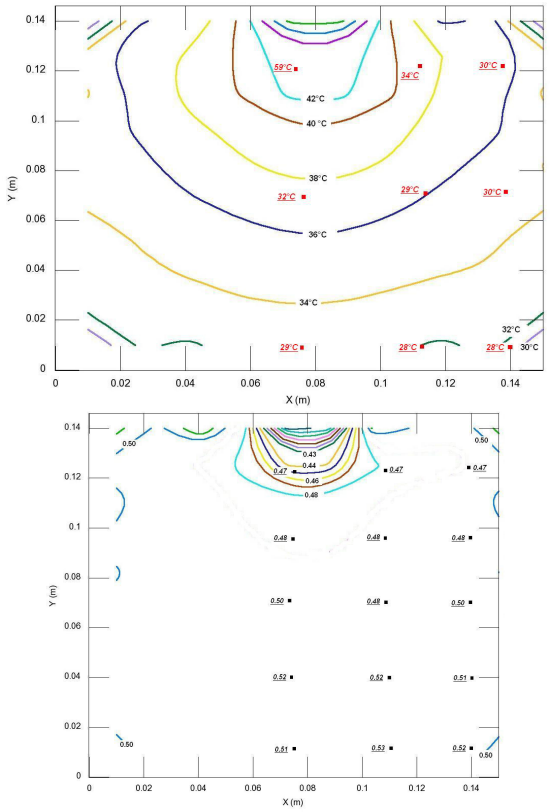

a. b.

Figure 10: Temperature (a) and saturation degree (b) of the compacted clay after 2 hours heating (dots: reference results from [78]; isochrones: numerical results obtained with Θ-Stock in the elastic domain of the THHMD model).

were similar to the ones of clay stone. The corresponding damage parameters were determined by Chiarelli and Shao [15]. With the chosen values of E, ν, C_0 and C_1 (Tab. 3), one may thus recommend: $g_M^{ref} = -1.414\,Pa$. The influence of the thermal resistance to cracking on the development of damage and on the evolution of the saturation degree are shown in Fig. 11 for some values of g_T. For the same reasons as mentioned in the previous thermo-mechanical study of nuclear waste storage, damage is isotropic. That is the reason why only one component of the damage tensor (Ω_{xx}) has been represented.

After two hours of heating, damage is mainly present around the heating source, away from the temperated boundaries. As could be expected, damage reaches higher values with higher g_T coefficients. When g_T parameter is low, the generated damage remains bounded to a few percents (Fig. 11.a), and the distribution of the degree of saturation is very similar to the one observed in an intact medium (Fig. 10.b and 11.b). The parametric study performed on g_T shows that if the medium is more densely cracked, the distribution of the degree of saturation is affected. As shown in Fig. 11.c,e,g, damage develops in the vicinity of the heating source, where tensile thermal strains reach their highest point. The permeability of the medium increases with damage. As a result, permeability becomes heterogeneous in the sample: permeability is higher near the source than at the bottom of the tank. In summary, near the source, the voids occupy more space (due to the presence of cracks), and permeability is higher. Therefore, near the source, liquid moves easily and capillary effects are reduced. If the sample had been drained, evaporation would have resulted in a fast drying of the sample from the top of the tank. In this example, the tank's walls are assumed to be impervious. Suction gets lower in the vicinity of the source than at the bottom of the tank. As a result, the degree of saturation becomes higher near the source than at the bottom of the tank, away from the source.

6.4. Study of the Influence of Initial Damage in a Full Scale Nuclear Waste Disposal (Parametric Study)

6.4.1. A Full Scale Heating Test in an Experimental Repository, with Unsaturated Buffers

The last numerical example presented in this paper aims at simulating a

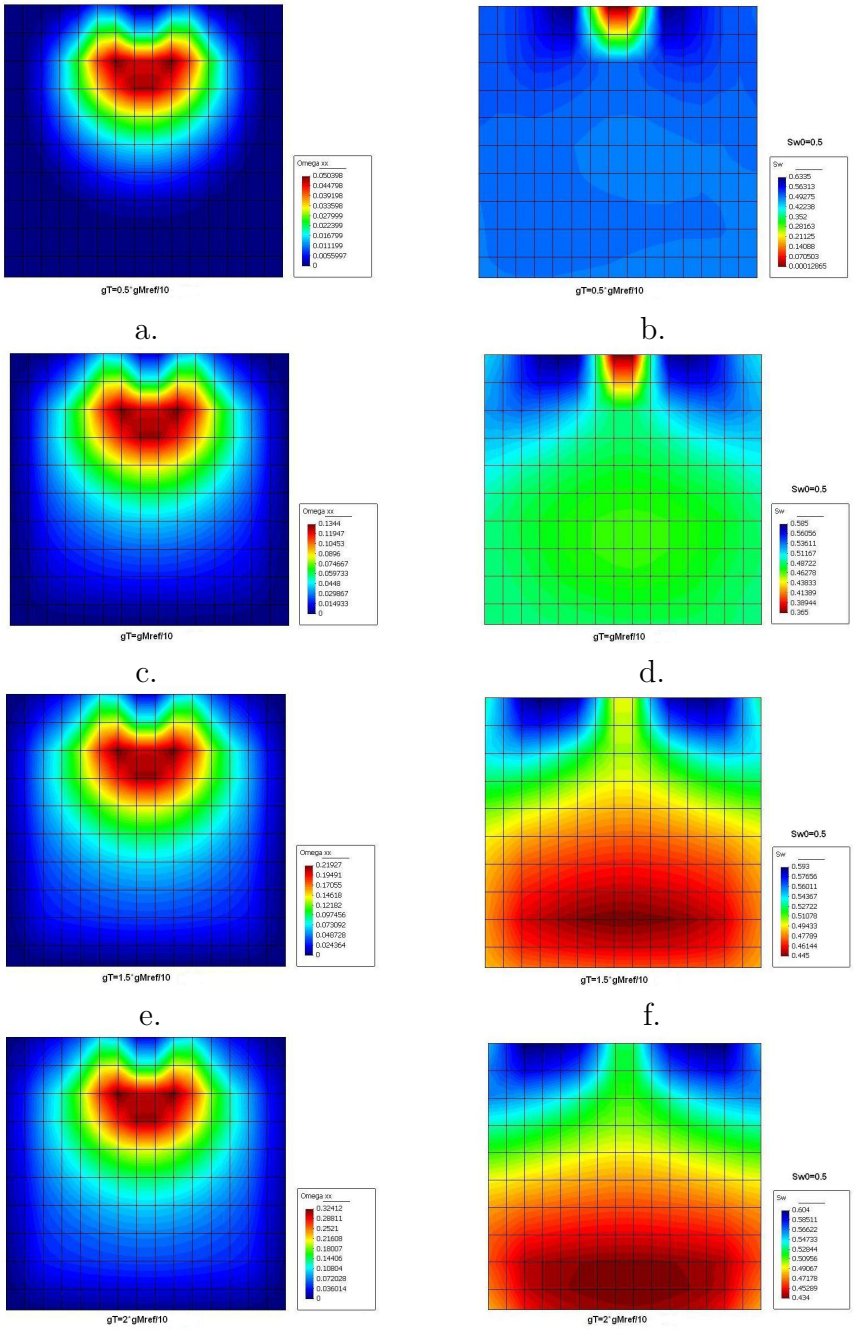

Figure 11: Influence of g_T on damage ($\Omega_{xx} = \Omega_{yy}$) and on the saturation degree, after 2 hours heating.

full-scale heating test performed in the experimental nuclear waste repository located at Kamaishi, in Japan. The reference data are taken from an article confronting the results of four numerical programs to experimental measurements [68]. Nuclear waste is modeled as a heating source stored in an initially saturated granite rock mass (GB, "geological barrier"). The nuclear package is disposed in a vertical well-bore, and is separated from the GB by a bentonite buffer (EB, "engineered barrier"). The initial saturation degree of bentonite is 0.635. The boundaries of the heater are assumed to be at $100\,^oC$ during 8.5 months (259 days). Then, the heating source is turned off, which means that a zero heat flux is imposed at the heater's boundaries. The behaviors of the engineered and of the geological barriers are observed during a relaxation period of 6 months (183 days). The initial temperature of the bentonite buffer and of the granite rock mass is $12.3\,^oC$.

The geometry and the loading type make it possible to study the problem in an axis-symmetric configuration. According to the numerical models presented in [68], the extent of the studied zone is 20 meters by 20 meters. A gallery provides an access to the well-bores. It is assumed that this gallery is watered by a shallow pool, so that $p_w = 0$ at the top of the granite bedrock. On the outer boundaries of the model, water pore pressure is hydrostatic. The authors assume that the air phase is static [68]. In Θ-Stock, fluid equilibrium is transient, so that it is only possible to approximate this static state. That is the reason why a zero air pore presure is initially imposed on all nodes. Then, a zero air pore pressure is imposed on the external boundaries of the model. The mesh and boundary conditions are represented in Fig. 12.

The reference article [68] presents a benchmark realized by four institutes. Each research team has used slightly different elastic thermo-mechanical parameters for the granite and bentonite materials under study. An average of the four values has been used in the input parameters to run the simulations with Θ-Stock. The damage parameters of the host massif are assumed to be similar to the ones of Vienne granite [43]. Eastern clay stone damage parameters [15] are affected to bentonite. Additional reference mechanical data are taken from [45] and [72]. Some retention properties which are not fully explained in the reference article have been taken from [39]. Standard values are adopted for specific heats and thermal conductivities. The choice of all the parameters is justified in detail in [1]. The main material data are summed up in Tab. 4 and Tab. 5.

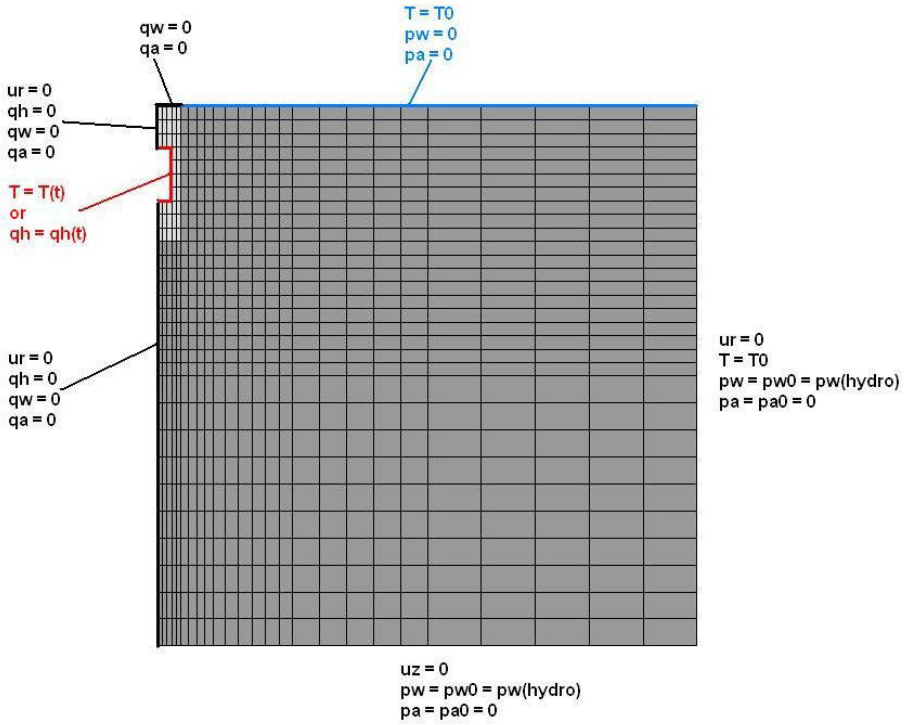

Figure 12: Boundary Conditions Adopted to Simulate the Heating Test Performed on Kamaishi Experimental Site [68].

Table 4: Elastic Material Parameters of Granite in Kamaishi's Heating Test [68].

E (Pa)	ν	β_s^0 (Pa)	β_T^0 (Pa)	C_0 (Pa)	C_1 (Pa)
$4.475 * 10^{10}$	0.3	$3.729 * 10^{11}$	$3.729 * 10^{11}$	$1.1 * 10^5$	$2.2 * 10^6$
k_{w0} $(m.s^{-1})$	α_w	$S_{w,r}$	α_{VG} (Pa^{-1})	n_{VG}	d_s
10^{-11}	0	0	10^{-5}	1.5	0
e_0	χ	k_{wdg}^{max} $(m.s^{-1})$	D_{dg}^{max} $(m^2.s^{-1})$	c_a (m^2)	α_a
0.00351	0.005	10^{-7}	10^{-5}	10^{-10}	0
α_0^*	C_{Ps}	C_{Pw}	C_{Pvap}	C_{Pa}	
$(^oC^{-1})$	$(J.kg^{-1}.^oC^{-1})$	$(J.kg^{-1}.^oC^{-1})$	$(J.kg^{-1}.^oC^{-1})$	$(J.kg^{-1}.^oC^{-1})$	
$-2.55 * 10^{-6}$	805	4180	1900	1006	
λ_s	λ_w	λ_a	h_{fg}		
$(W.m^{-1}.^oC^{-1})$	$(W.m^{-1}.^oC^{-1})$	$(W.m^{-1}.^oC^{-1})$	$(J.kg^{-1})$		
3	0.6	0.0258	$2.5 * 10^6$		

Table 5: Elastic Material Parameters of Bentonite in Kamaishi's Heating Test [68].

E (Pa)	ν	β_s^0 (Pa)	β_T^0 (Pa)	C_0 (Pa)	C_1 (Pa)
$1.175 * 10^8$	0.35	$3.729 * 10^{11}$	$3.729 * 10^{11}$	$2.3 * 10^{-4}$	$5.2 * 10^{-3}$
k_{w0} $(m.s^{-1})$	α_w	$S_{w,r}$	α_{VG} (Pa^{-1})	n_{VG}	d_s
$2 * 10^{-13}$	0	0	$2 * 10^{-7}$	2	0
e_0	χ	k_{wdg}^{max} $(m.s^{-1})$	D_{dg}^{max} $(m^2.s^{-1})$	c_a (m^2)	α_a
0.637	0.005	$2 * 10^{-9}$	$2 * 10^{-7}$	10^{-10}	0
α_0^*	C_{Ps}	C_{Pw}	C_{Pvap}	C_{Pa}	
$(^oC^{-1})$	$(J.kg^{-1}.^oC^{-1})$	$(J.kg^{-1}.^oC^{-1})$	$(J.kg^{-1}.^oC^{-1})$	$(J.kg^{-1}.^oC^{-1})$	
$-2.55 * 10^{-5}$	1250	4180	1900	1006	
λ_s	λ_w	λ_a	h_{fg}		
$(W.m^{-1}.^oC^{-1})$	$(W.m^{-1}.^oC^{-1})$	$(W.m^{-1}.^oC^{-1})$	$(J.kg^{-1})$		
1.15	0.6	0.0258	$2.5 * 10^6$		

6.4.2. Verification of the Results in the Absence of Damage

The reference article [68] focuses on coupling effects and deals with elastic models. In the real experimental site, horizontal fractures have been observed in the granite rock mass. Some of the simulations presented in the reference paper take these fractures into account by considering them as a geomaterial endowed with a specific hydraulic transmissivity. Some other simulations ignore the presence of initial damage. The first step of our work consists in simulating Kamaishi heating test in an elastic intact geological massif. This first study aims at verifying the results provided by Θ-Stock in a complex problem, involving two different porous materials that may interact due to coupled thermo-hydro-mechanical effects. The second step of our work will consist in accounting for initial damage, as explained in the following paragraph.

The evolution of temperature (Fig. 13) in the elastic geological and engineered barriers are described in Tab. 4 and Tab. 5. The trends and orders of magnitude are satisfactory, with maximal errors amounting to around 10%. The main differences are observed in transient stages and may thus be attributed to a problem of kinetics, as stated in the two preceding examples. The underestimated bentonite temperature may be due to the differences of the models for the specific heat and for the thermal conductivity of the

barriers. The authors of the reference article [68] chose to set a dependence of C_{Ps} and λ_s on the saturation degree. In Θ-Stock, heat transfer is modeled a bit differently. The various constituents are assumed to be in parallel. As a consequence, the volumetric fractions of each constituent (solid, liquid water, vapor and gaseous air) are used to weight the sum of the constituents specific heats (equation 73) and thermal conductivities (equation 65) in the computation of the global medium's thermal properties. Not only the degree of saturation but also porosity play a role in the transfer of heat in the porous medium. In other words, water content $\theta_w = n\,S_w$ plays an important role in the heat transfer model adopted in Θ-Stock.
The saturation degree of the engineered barrier follows a satisfactory trend. At the frontier with the granite bedrock (Fig. 14.a), the bentonite buffer reaches a 0.97 saturation degree in approximately two hundred days. This quasi-saturated state is maintained during the whole relaxation period, which corresponds to the reference results [68]. At the boundary between the heating source and the engineered barrier (Fig. 14.b), the saturation degree falls to almost 0 in approximately one hundred days, which is in agreement with the trends reported in [68]. Then, the reference saturation degree increases after the heating period, while Θ-Stock predicts a stabilization around $S_w = 0$, even during the relaxation period. This difference may be attributed to the way C_{PT} and λ_T are modeled, as explained above.

6.4.3. Influence of the Presence of Cracks Before Waste Disposal

As mentioned before, Kamaishi's granite host massif is fractured. To be closer to the real conditions, the heating test is now simulated in an initially damaged geological barrier. In the THHMD model, the horizontal fracture present in the bedrock is accounted for by setting a non-zero value for the vertical component of the initial damage tensor, as shown in Fig. 15. The loading process and the material parameters given in Tab. 4 and in Tab. 5 are kept the same as in the previous numerical study. The evolution of the saturation degree in both the engineered and the geological barriers is shown in Fig. 16 for an initially intact rock mass, and in Fig. 17 for an initially damaged host rock. The presence of initial damage strongly affects fluid exchanges. In the particular case presented here, initial cracking results in a strong desaturation of the engineered barrier at the beginning of the heating period (Fig. 17, after 10 days). After 6 months of relaxation (i.e. after 442 days of test), the extent of the desaturation zone is much wider in

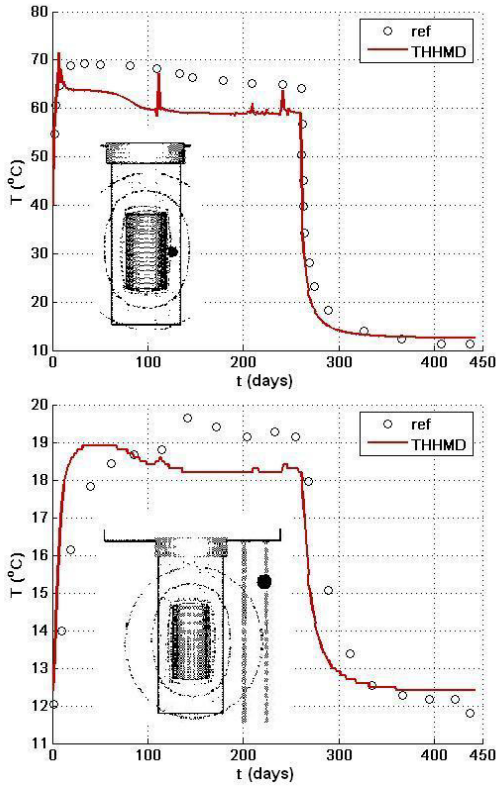

a. b.

Figure 13: Temperature evolution with intact elastic geological and engineered barriers. a. In bentonite, at equal distances from the heating source and from the bedrock, at mid-height of the heating device. b. In the bedrock, near the engineered barrier.

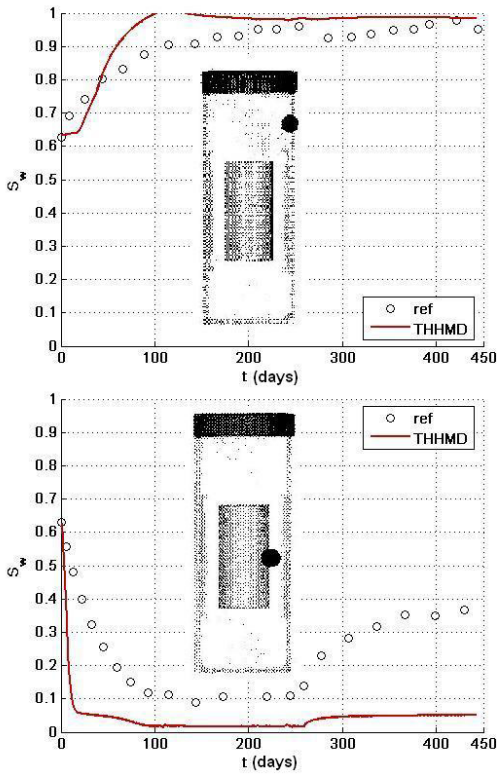

a. b.

Figure 14: Saturation degree evolution with intact elastic geological and engineered barriers. a. In the bentonite engineered barrier, at approximately 1 centimeter from the geological massif, above the heating device. b. In the contact zone between the heating source and the engineered barrier, at mid-height of the heating device.

the initially damaged rock mass than in the initially intact host rock. The geological barrier is desaturated up to five meters away from the heating source (Fig. 17, after 442 days).

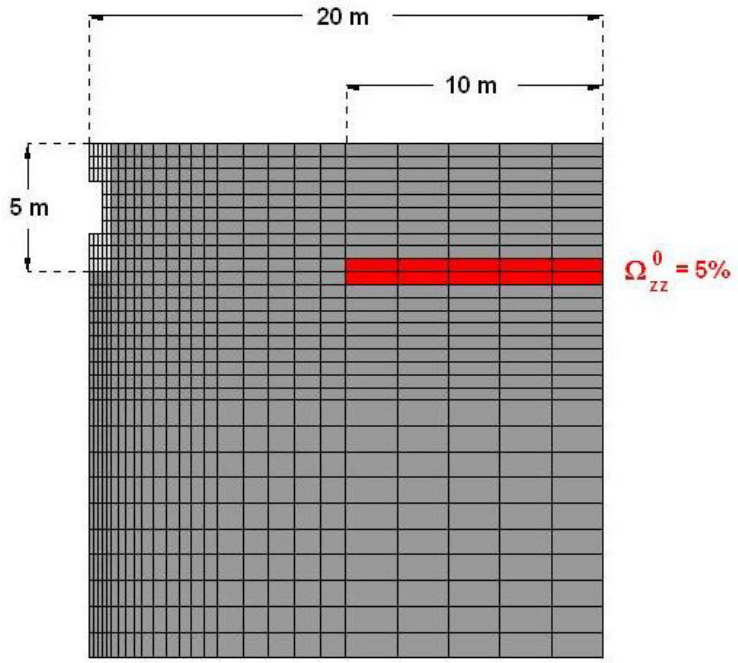

Figure 15: Study of the Nuclear Waste Storage Problem on Kamaishi Site. Initially Damaged Configuration: One 10-Meter Wide Horizontal Fracture Plane.

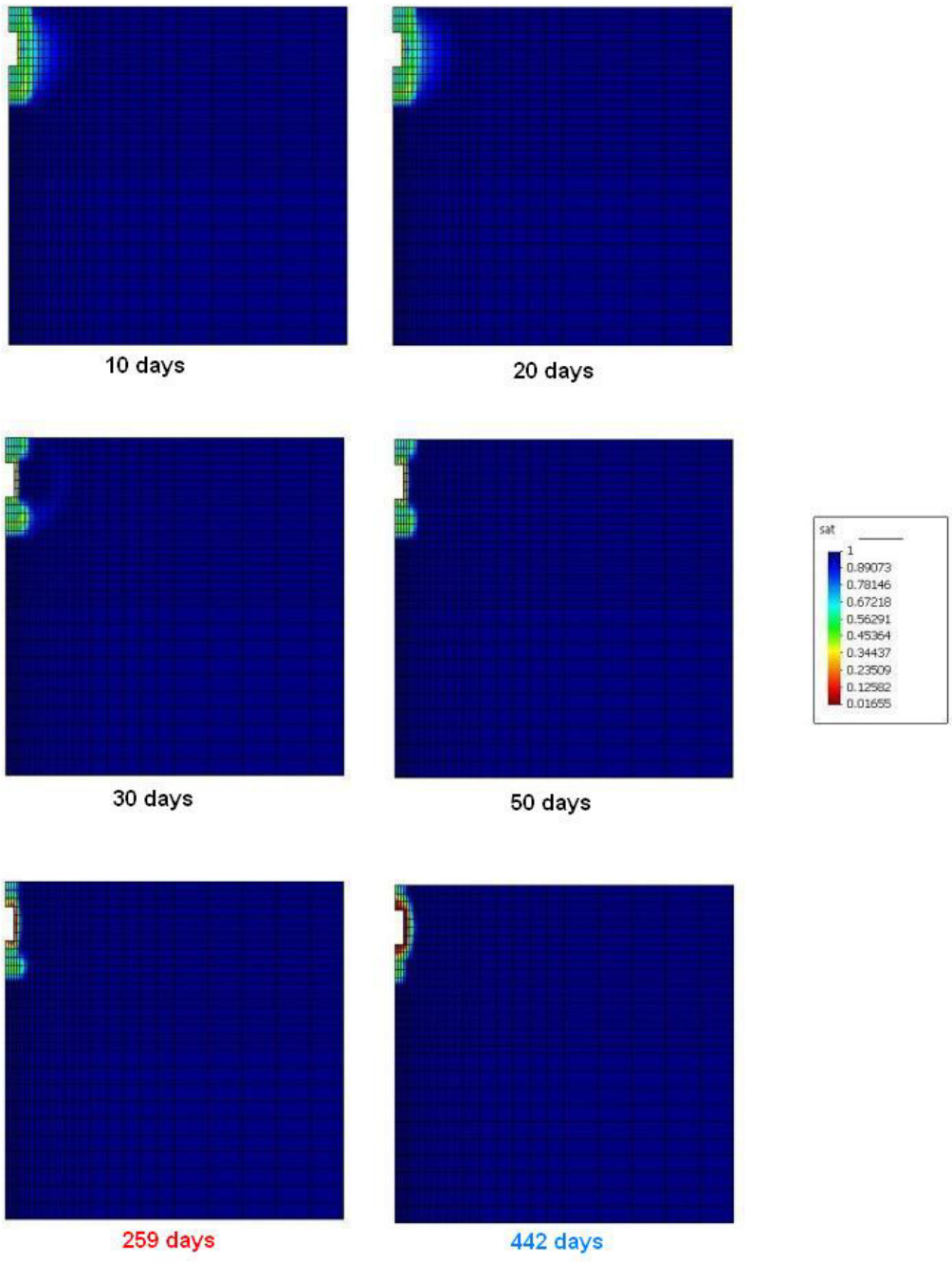

Figure 16: Evolution of the saturation degree in space and time for the nuclear waste storage problem on Kamaishi site. Initially intact granite bedrock.

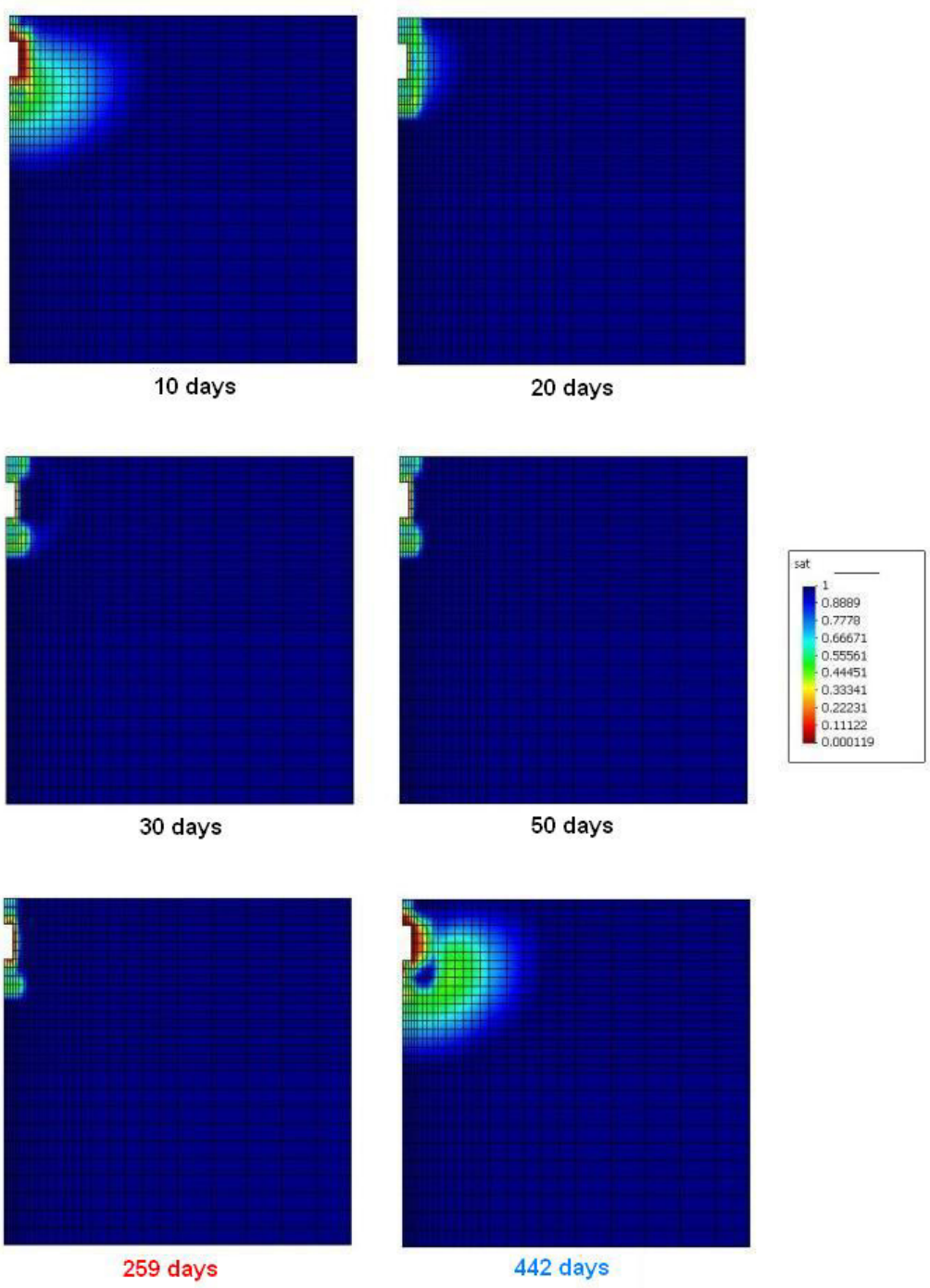

Figure 17: Evolution of the saturation degree in space and time for the nuclear waste storage problem on Kamaishi site. Initially damaged granite bedrock (with one 10-meter wide horizontal fracture plane).

7. CONCLUSION

The damage model presented in this article (named "THHMD" model) is dedicated to non-isothermal unsaturated porous media. Assuming that the solid phase of the medium is incompressible, the model is formulated by means of three independent state variables: mechanical strains, capillary strains and thermal strains (respectively conjugate to net stress, suction and thermal stress). The damage variable is a second-order tensor, representing crack density in the three principal stress directions. Stress/strain relationships are derived from Helmholtz free energy, which is assumed to be the sum of damaged elastic potentials and "crack-closure energies". The Principle of Equivalent Elastic Energy is used to get the damaged mechanical stiffness tensor, the damaged capillary modulus and the damaged thermal expansion coefficient. Damage is assumed to grow with tensile strains generated by the variations of net stress, suction and temperature. The model accounts for water phase changes. Gas is thus a mixture of dry air and vapor. Specific conductivities related to damage are introduced to account for the effects of cracking on the intensification and on the orientation of liquid water and vapor flows. Both damaged conductivities depend on a specific internal length parameter. Air and heat flow equations are kept the same as in an intact porous medium. Damage is accounted for indirectly, through porosity and saturation degree variations.

The THHMD model has been programmed in Θ-Stock Finite Element code. The model has been validated on bare mechanical problems. In this paper, only a few results are presented. The simulation of triaxial compression test on dry sandstone shows that the mechanical predictions of the THHMD model match the experimental measurements found in the literature. Very few reference studies dealing with both damage and thermal effects in unsaturated porous media exist in the literature. That is the reason the other numerical examples presented in this article are based on parametric studies on damage, and not on validation tests. Three examples, related to the study of nuclear waste disposals, are presented: 1. a one-dimensional thermo-mechanical heating test in granite, 2. a heating test performed at the lab scale in deformable unsaturated compacted clay, and 3. a full scale heating test realized in Kamaishi's experimental facility. For each case study, one simulation has first been run in the absence of damage, and the results have been compared to the ones presented in reference articles. In this first

step, the response of the program in fully coupled problems has been examined. Some temperature discrepancies have been noted in the transient stages of heat transfer. Overall, the results provided by the program follow the expected trends with the appropriate orders of magnitude. In a second step, a parametric study of damage has been performed on each example. In example 1 (thermo-mechanical heating test), it is verified that damage and irreversible strains grow with the parameter representing the resistance to thermal cracking (g_T). In example 2 (heating of a deformable unsaturated clay sample), the damage effects observed on permeability are in agreement with the theoretical formulation of the model. In the vicinity of the heating source, the material is more densely cracked and becomes more permeable. Capillary effects get lower than in the colder zones. As a result, cracked samples tend to dry near the tank walls, whereas the intact sample dries close to the heating source. In example 3 (full scale heating test in an experimental facility), a horizontal crack plane is modeled by setting a non zero initial damage field. The consequences on the degree of saturation of the bentonite buffer and of the host rock are huge, which demonstrates the importance of the assessment of the EDZ before waste disposal. The engineering problems tackled in this article are realistic. Several types of loading and boundary conditions have been investigated. Therefore, the effects of thermal damage have been thoroughly studied. The works presented in this article only constitute the first step of a long-term research project on damage poromechanics. The authors are currently improving the heat and mass transfer models implemented in Θ-Stock program. Experimental data remain necessary to scale capillary and thermal damage effects in porous geomaterials.

APPENDIX 1: COMPUTATION OF THE TIME DERIVATIVES INVOLVED IN THE MOISTURE MASS EQUATION

It is recalled that, with the soil mechanics convention, the assumption of solid phase incompressibility results in:

$$\frac{\partial n}{\partial t} = -\delta : \frac{\partial \epsilon}{\partial t} \tag{81}$$

The equation of the state surface of the saturation degree 42 is used in order to express $\frac{\partial S_w}{\partial t}$:

$$\left\{\begin{array}{l} \frac{\partial S_w}{\partial t} \;=\; g_2 \frac{\partial s}{\partial t} \;+\; g_3 \frac{\partial T}{\partial t} \\ \\ g_2 = \frac{\partial S_w}{\partial s} \;=\; \left\{\begin{array}{l} (1-n)\alpha^n (1-S_{w,r}) exp\left(d_s (T-T_0)\right) \left(1+(\alpha\, s)^n\right)^{\frac{1-2n}{n}} \; s^{n-1} \quad if \quad s \geq 0 \\ \\ 0 \quad if \quad s < 0 \end{array}\right. \\ \\ g_3 = \frac{\partial S_w}{\partial T} \;=\; d_s \, S_w \end{array}\right. \tag{82}$$

The time variation of the density of liquid water is written as:

$$\left\{\begin{array}{l} \frac{\partial \rho_w}{\partial t} \;=\; \beta_P \frac{\partial p_w}{\partial t} \;+\; \beta_T \frac{\partial T}{\partial t}, \\ \\ \beta_P = \frac{\partial \rho_w}{\partial p_w} = 5.10^{-10}\, m^{-2}.s^2, \quad \beta_T = \frac{\partial \rho_w}{\partial T} = -2.10^{-4}\, kg.m^{-3}.{}^oC^{-1} \end{array}\right. \tag{83}$$

Using the formula of Philip and de Vries [64] for the vapor density 52, with the preceding assumption $\frac{\partial h(\theta_w,T)}{\partial T} \simeq 0$, the time derivation of ρ_{vap} may be computed as:

$$\begin{array}{l} \frac{\partial \rho_{vap}}{\partial t} \;=\; -A_n \, S_w \, \delta \;:\; \frac{\partial \epsilon}{\partial t} \;-\; A_n \, n \, g_2 \, \frac{\partial p_w}{\partial t} \;+\; A_n \, n \, g_2 \, \frac{\partial p_a}{\partial t} \\ + \left(A_{\rho_0} \, \rho_{vap}\left(\theta_w, T\right) \;+\; A_n \, n \, g_3\right) \, \frac{\partial T}{\partial t} \end{array} \tag{84}$$

A_n and A_{ρ_0} are computed by using equations 52, 53, 34 and 35:

$$\left\{\begin{array}{l} A_n \;=\; \frac{\partial \rho_{vap}}{\partial \theta_w} \;=\; \left\{\begin{array}{l} -\frac{\rho_{vap}}{n \rho_w R_{vap} T} \frac{\sigma(T)}{\sigma(T_{ref})} \frac{\partial s}{\partial S_w} \quad if \quad s \geq 0 \\ \\ 0 \quad if \quad s < 0 \end{array}\right. \\ \\ A_{\rho_0} \;=\; \frac{1}{\rho_{vap}} \frac{\partial \rho_{vap}}{\partial T} \;=\; \frac{1}{\rho^0_{vap}} \frac{d\rho^0_{vap}}{dT} \;=\; \frac{4975.9}{(T+273.15)^2} \end{array}\right. \tag{85}$$

For $s \geq 0$, $\frac{\partial s}{\partial S_w}$ is determined by inverting the equation of the state surface of the saturation degree 42:

$$\begin{array}{l} \frac{\partial s}{\partial S_w}\big|_{s\geq 0} \;=\; \frac{exp(-d_s(T-T_0))}{\alpha\,(1-n)(1-S_{w,r})} \left[\frac{S_w \, exp(-d_s(T-T_0)) - S_{w,r}}{1-S_{w,r}}\right]^{\frac{2n-1}{1-n}} \\ \\ \qquad \times \left[\left[\frac{S_w \, exp(-d_s(T-T_0)) - S_{w,r}}{1-S_{w,r}}\right]^{\frac{n}{1-n}} - 1\right]^{\frac{1-n}{n}} \end{array} \tag{86}$$

References

[1] Arson C. Etude théorique et numérique de l'endommagement thermo-hydro-mécanique des milieux poreux non saturés. *PhD thesis (in French), Ecole Nationale des Ponts et Chaussées, Paris, France* 2009.

[2] Arson C, Gatmiri B. On damage modelling in unsaturated clay rocks. *Physics and Chemistry of the Earth* 2008; **33**:S407–S415.

[3] Arson C, Gatmiri B. A mixed damage model for unsaturated porous media. *Comptes-Rendus de l'Acadmie des Sciences de Paris, section Mcanique* 2009; **337**:68–74.

[4] Arson C, Gatmiri B. Parametric study on the performance of a THM damage model for unsaturated porous media. *1st International Symposium on Computational Geomechanics, Juan-les-Pins, France* 2009; 553–562.

[5] Arson C, Gatmiri B. Numerical study of a thermo-hydro-mechanical damage model for unsaturated porous media. *Annals of Solid and Structural Mechanics* 2010; **1**:59–78.

[6] Askes H, Sluys LJ. Explicit and implicit gradient series in damage mechanics. *Euro. J. Mech. Solids* 2002. **21**:379–390.

[7] Bazant ZP. Why continuum damage is nonlocal: micromechanics arguments. *J. Eng. Mec. ASCE* 1991; **117**(5):1070–1087.

[8] Bazant ZP, Jirasek M. Nonlocal integral formulations of plasticity and damage: survey of progress. *J. Eng. Mec. ASCE* 2002; **128**(11):1119–1149.

[9] Bazant ZP, Ozbolt J. Nonlocal microplane model for fracture, damage, and size effect in structures. *J. Eng. Mech. ASCE* 1990. **116**(11):2485–2505.

[10] Blumling P, Bernier F, Lebon P, Martin CD. The excavation damaged zone in clay formations time-dependent behaviour and influence on performance assessment. *Physics and Chemistry of the Earth* 2007; **32**(8-14):588–599.

[11] Bonin B. Deep geological disposal in argillaceous formations : studies at the Tournemire test site. *J. of Contaminant Hydrology* 1998; **35**:315–330.

[12] Bourgeois F, Burlion N, Shao JF. Modelling of elastoplastic damage in concrete due to desiccation shrinkage. *Int. J. Num. Anal. Meth. Geomech.* 2002; **26**:759–774.

[13] Carter JP, Booker JR. Finite element analysis of coupled thermoelasticity. *Computers and Structures* 1989; **31**(1):75–80.

[14] Chambon R, Caillerie D, Tamagnini C. A strain space gradient plasticity theory for finite strain. *Comput. Meth. Appl. Mech. Eng.* 2004; **193**:2797–2826.

[15] Chiarelli AS, Shao JF. Modélisation élastoplastique couplée à l'endommagement anisotrope induit pour des argilites. *Revue Francaise de Génie Civil* 2002; **6**(1):115–130.

[16] Cicekli U, George Z. Voyiadjis GZ, Abu Al-Rub RK. A plasticity and anisotropic damage model for plain concrete. *International Journal of Plasticity* 2007; **23**:1874–1900.

[17] Collins IF, Houlsby GT. Application of thermomechanical principles to the modelling of geotechnical materials. *Proceedings of the Royal Society, Mathematical, Physical and Engineering Sciences* 1997; **453**(1964):1975–2001.

[18] Cordebois JP, Sidoroff F. Endommagement anisotrope en élasticité et plasticité. *Journal de Mécanique théorique et appliquée* 1982; 45–60.

[19] Coussy O, Dangla P. Approche énergétique du comportement des sols non saturés. in *Mécanique des sols non saturés.* Hermès, 2002. 137–174.

[20] Dangla P, Malinsky L, Coussy O. Plasticity and imbibition-drainage curves for unsaturated soils : a unified approach. *Proc. Numerical Models in Geomechanics* 1997;141–146.

[21] de Borst R, Pamin J, Geers MGD. On coupled gradient-dependent plasticity and damage theories with a view to localization analysis. *Eur. J. Mech. A/Solids* 1999. **18**:939–962.

[22] de Vree JHP, Brekelmans WAM, van Gils MAJ. Comparison of non local approaches in continuum damage mechanics. *Comput. Struct.* 1995. **55** (4):581–588.

[23] Dragon A, Halm D. Modélisation de l'endommagement par mésofissuration : comportement unilatéral et anisotropie induite. *C.R. Acad. Sci. Paris, T322, Série IIb* 1996; 275–282.

[24] Dragon A, Halm D, Desoyer Th. Anisotropic damage in quasi-brittle solids: modelling, computational issues and applications. *Comput. Methods Appl. Mech. Engrg.* 2000; **183**:331–352.

[25] Durner W. Hydraulic conductivity estimation for soils with heterogeneous pore structure. *Water Resour. Res.* 1994; **30**(2):211–223.

[26] Ewen J, Thomas HR. Heating unsaturated medium sand. *Géotechnique* 1989; **39**(3):455–470.

[27] Farouki OT. Thermal properties of soils. *Trans Tech Publications, series on Rock and Soil Mechanics* 1986; **11**:20–55,102–119.

[28] Fredlund DG, Morgenstern NR. Stress state variables for unsaturated soils. *J. of the Soil Mechanics and Foundations Division* 1977; 447–466.

[29] Frémond M, Nedjar B. Damage, gradient of damage and principle of virtual power. *Int. J. Solids Struct.* 1996; **33**(8):1083–1103.

[30] Gatmiri B. Framework of a non linear fully coupled thermo-hydro-mechanical behaviour of unsaturated porous media. *Keynote lecture of the 3rd Iranian International Conference on Geotechnical Engineering and Soil Mechanics, Teheran, Iran* 2002.

[31] Gatmiri B. Non Linear Behaviour Of A Multiphase Engineering Barrier In Nuclear Waste Disposal. *Proc. 16th ICSMGE, Osaka, Japan* 2005; 2261–2264.

[32] Gatmiri B, Arson C. Theta-Stock, a powerful tool for thermohydromechanical behaviour and damage modelling of unsaturated porous media. *Computers and Geotechnics* 2008; **35**(6):890–915.

[33] Gatmiri B, Hoor A. Excavation effect on the thermo-hydro-mechanical behaviour of a geological barrier. *Physics and Chemistry of the Earth* 2007; **32**(8-14):947–956.

[34] Gatmiri B, Seyedi M, Delage P, Fry FF. A new suction-based mathematical model for thermo-hydro-mechanical behavior of unsaturated porous media. *Proceedings of the 6th International Symposium on Numerical Models in Geomechanics, NUMOG VI, Quebec, Canada* 1997; 291–296.

[35] Gawin D, Pesavento F, Schrefler BA. Modelling of hygro-thermal behaviour and damage of concrete at temperature above the critical point of water. *Int. J. Numer. Anal. Meth. Geomech.* 2002; **26**:537–562.

[36] Gawin D, Pesavento F, Schrefler BA. Simulation of damage-permeability coupling in hygro-thermo-mechanical analysis of concrete at high temperature. *Commun. Numer. Meth. Engng* 2002; **18**:113–119.

[37] Gawin D, Pesavento F, Schrefler BA. Modelling of hygro-thermal behaviour of concrete at high temperature with thermo-chemical and mechanical material degradation. *Comput. Methods Appl. Mech. Engrg.* 2003; **192**:1731–1771.

[38] Gawin D, Pesavento F, Schrefler BA. Modeling deterioration of cementitious materials exposed to calcium leaching in non-isothermal conditions. *Comput. Methods Appl. Mech. Engrg.* 2009; **198**:3051–3083.

[39] Gens A, Garcia-Molina AJ, Olivella S, Alonso EE, Huertas F. Analysis of a full scale in situ test simulating repository conditions. *International Journal for Numerical and Analytical Methods in Geomechanics* 1998; **22**:515–548.

[40] Gwo JP, Jardine PM, Wilson GV, Yeh GT. A multiple-pore-region concept to modeling mass transfer in subsurface media. *J. Hydrol.* 1995; **164**:217–237.

[41] Halm D, Dragon A. Modlisation de l'endommagement par mso-fissuration : comportement unilatral et anisotropie induite. *C.R. Acad. Sci. Paris* 1996; **T322**(IIb):275–282.

[42] Halm D, Dragon A. An anisotropic model of damage and frictional sliding for brittle materials. *Eur. J. Mech. A/ Solids* 1998; **17**(3):439–460.

[43] Halm D, Dragon A. Modélisation de l'endommagement par mésofissuration du granite. *Revue Française de Génie Civil* 2002. **6**(1): 21–33.

[44] Hansen NR, Schreyer HL. A thermodynamically consistent framework for theories of elastoplasticity coupled with damage. *Int. J. Solids and Structures* 1994; **31**(3):359–389.

[45] Homand F, Chiarelli AS, D. Hoxha D. Caractéristiques physiques et mécaniques du granite de la Vienne et de l'argilite de l'Est. *Revue Française de Génie Civil* 2002. **6**(1): 11–20.

[46] Houlsby GT. The work input to an unsaturated granular material. *Geotechnique* 1997; **47**(1):193–196.

[47] Jenab B. Etude numérique de la modélisation thermo-élasto-plastique des sols non saturés. *PhD thesis, Ecole Nationale des Ponts et Chaussées, Paris, France* 2000.

[48] Jia Y, Song XC, Duveau G, Su K, Shao JF. Elastoplastic damage modelling of argillite in partially saturated condition and application. *Phys. Chem. Earth* 2007; **32**:656–666.

[49] Jirasek M. Nonlocal models for damage and fracture: comparison of approaches. *Int. J. Solids Struct.* 1998. **35**(3132):4133–4145.

[50] Kachanov M. Effective elastic properties of cracked solids: critical review of som basic concepts. *Appl. Mech. Rev.* 1992; **45**(8):304–335.

[51] Kuhl D, Bangert F, Meschke G. Coupled chemo-mechanical deterioration of cementitious materials. Part I: Modeling. *International Journal of Solids and Structures* 2004; **41**:15–40.

[52] Kuhl D, Bangert F, Meschke G. Coupled chemo-mechanical deterioration of cementitious materials. Part II: Numerical methods and simulations. *International Journal of Solids and Structures* 2004; **41**:41–67.

[53] Lasry D, Belytschko T. Localization limiters in transient problems. *Int. J. Solids Struct.* 1988; **24**(6):581–597.

[54] Lemaître J, Desmorat R. *Engineering Damage Mechanics. Ductile, creep, fatigue and brittle failure.* Springer - Verlag, Berlin Heidelberg, 2005.

[55] Maleki K. Modélisation numérique du couplage entre l'endommagement et la perméabilité des roches. Application à l'étude des ouvrages de stockage souterrain. *PhD thesis (in French), Ecole Nationale des Ponts et Chaussées, Paris, France* 2004.

[56] Maleki K, Pouya A. Numerical Simulation of Damage-Permeability Relationship in Brittle Geomaterials. *Computers and Geotechnics* 2010; **37**:619–628.

[57] Martino JB, Chandler NA. Excavation-induced damage studies at the Underground Research Laboratory. *Int. J. Rock Mech. and Min. Sci.* 2004; **41**:1413–1426.

[58] Menzel A, Steinmann P. A theoretical and computational framework for anisotropic continuum damage mechanics at large strains. *Int. J. Solids Struct.* 2001; **38**:9505–9523.

[59] Mertens J, Bastiaens W, Dehandschutter B. Characterization of induced discontinuities in the Boom Clay around the underground excavations (URF, Mol, Belgium). *Appl. Clay Science* 2004; **26**:413–428.

[60] Ortiz M. A constitutive theory for the inelastic behaviour of concrete. *Mech. Mater.* 1985; **4**:67–93.

[61] Othmer M, Diekkrger B, Kutilek M. Bimodal porosity and unsaturated hydraulic conductivity. *Soil Sci.* 1991; **152**(3):139–150.

[62] Pamin J. Gradient plasticity and damage models: a short comparison. *Comput. Mater. Sci.* 2005. **32**:472–479.

[63] Pesavento F, Gawin D, Schrefler BA. Modeling cementitious materials as multiphase porous media: theoretical framework and applications. *Acta Mechanica* 2008; **201**:313–339.

[64] Philip J.R., de Vries, D.A. Moisture Movement in Porous Materials under Temperature Gradients. *Transactions, American Geophysical Union* 1957; **38**(2):222–232.

[65] Pires-Domingues SM, Costa-Mattos H, Rochinha FA. Modelling of nonlinear damage on elastic brittle materials. *Mech. Res. Commun.* 1998; **25**(2):147–153.

[66] Preece RJ. The measurement and calculation of physical properties of cable bedding sands. Part 2: Specific thermal capacity, thermal conductivity, and temperature ratio across "air" filled pores. *Technical Report Laboratory note, Central Electricity Generating Board, London, UK* 1975; RD/L/N 231/74.

[67] Pruess K, Wang JSY, Tsang YW. On thermohydrologic conditions near high-level nuclear wastes emplaced in partially saturated fractured tuff. 2. Effective continuum approximation. *Water Resour. Res.* 1990; **26**(6):1249–1261.

[68] Rutqvist J, Borgesson L, Chijimatsu M, Nguyen TS, Jing L, Noorishad J, Tsang CF. Coupled thermo-hydro-mechanical analysis of a heater test in fractured rock and bentonite at Kamaishi Mine - comparison of field results to predictions of four finite element codes. *International Journal of Rock Mechanics and Mining Sciences* 2001; **38**:129–142.

[69] Schrefler BA, Pesavento F. Multiphase flow in deforming porous material. *Computers and Geotechnics* 2004; **31**:237–250.

[70] Shao JF, Ata N, Ozanam O. Study of desaturation and resaturation in brittle rock with anisotropic damage. *Engineering geology* 2005; **81**:341–352.

[71] Shao JF, Duveau G, Bourgeois F, Chen WZ. Elastoplastic damage modeling in unsaturated rocks and applications. *Int. J. Geomech.* 2006; **6**(2):119–130.

[72] Shao JF, Zhou H, Chau KT. Coupling between anisotropic damage and permeability variation in brittle rocks. *International Journal for Numerical and Analytical Methods in Geomechanics* 2005; **29**:1231–1247.

[73] Svedberg T, Runesson K. A thermodynamically consistent theory of gradient-regularized plasticity coupled to damage. *Int. J. Plasticity* 1997; (6-7):669–696.

[74] Swoboda G, Yang Q. An energy-based damage model of geomaterials 1. Formulation and numerical results. *Int. J. Solids and Struct.* 1999; **36**:1719–1734.

[75] Tsang CF, Bernier F, Davies C. Geohydromechanical processes in the Excavation Damaged Zone in crystalline rock, rock salt, and indurated and plastic clays - in the context of radioactive waste disposal. *Int. J. Rock Mech. and Min. Sci.* 2005; **42**:109–125.

[76] Van Genuchten MTh. A closed-form equation for predicting the hydraulic conductivity of unsaturated soils. *Soil Science Society of America Journal* 1980; **44**:892–898.

[77] Vardoulakis I, Sulem J. *Bifurcation Analysis in Geomechanics, chapter 10: Second-grade plasticity theory for geomaterials, Blackie Academic and Professional* 1995; :382–425.

[78] Villar MV, Cuevas J, Fernandes AM, Martin PL. Effects of the interaction of heat and water flow in compacted bentonite. *Proceedings of the First International Workshop on the Thermodynamics of Clays and Clay Barriers (ISMES), Bergamo, Italy* 1993.

[79] Vogel T, Gerke HH, Zhang R, Van Genuchten MT. Modeling flow and transport in a two-dimensional dual-permeability system with spatially variable hydraulic properties. *J. Hydrol.* 2000; **238**:78–89.

[80] Zimmerman RW, Hadgu T, Bodvarsson GS. A new lumped-parameter model for flow in unsaturated dual-porosity media. *Adv. Water Resour.* 1996; **19**(5):317–327.